Research Paper

GEOSPHERE

GEOSPHERE; v. 14, no. 5

https://doi.org/10.1130/GES01678.1

18 figures; 6 tables; 1 supplemental file

CORRESPONDENCE: lithia35@gmail.com

CITATION: Witkosky, R., and Wernicke, B.P., 2018, Subsidence history of the Ediacaran Johnnie Formation and related strata of southwest Laurentia: Implications for the age and duration of the Shuram isotopic excursion and animal evolution: Geosphere, v. 14, no. 5, p. 2245–2276, https://doi.org/10.1130/GES01678.1.

Science Editor: Raymond M. Russo
Associate Editor: Christopher J. Spencer

Received 10 February 2018
Revision received 30 April 2018
Accepted 19 July 2018
Published online 14 August 2018

Subsidence history of the Ediacaran Johnnie Formation and related strata of southwest Laurentia: Implications for the age and duration of the Shuram isotopic excursion and animal evolution

Rebecca Witkosky and Brian P. Wernicke
Division of Geological and Planetary Sciences, California Institute of Technology, 1200 E. California Boulevard, MC 170-25, Pasadena, California 91125, USA

ABSTRACT

The Johnnie Formation and associated Ediacaran strata in southwest Laurentia are ~3000 m thick, with a Marinoan cap carbonate sequence at the bottom, and a transition from Ediacaran to Cambrian fauna at the top. About halfway through the sequence, the Shuram negative carbon isotopic excursion occurs within the Rainstorm Member near the top of the Johnnie Formation, followed by a remarkable valley incision event. At its type locality in the northwest Spring Mountains, Nevada, the Johnnie lithostratigraphy consists of three distinctive sand-rich intervals alternating with four siltstone/carbonate-rich intervals, which appear correlative with other regional Johnnie Formation outcrops. Carbon isotope ratios in the sub–Rainstorm Member part of the Johnnie Formation are uniformly positive for at least 400 m below the Shuram excursion and compare well with sub–Shuram excursion profiles from the Khufai Formation in Oman. There is historical consensus that the Johnnie and overlying formations were deposited on a thermally subsiding passive margin. Following previous authors, we used Paleozoic horizons of known biostratigraphic age to define a time-dependent exponential subsidence model, and extrapolated the model back in time to estimate the ages of the Shuram excursion and other prominent Ediacaran horizons. The model suggests that the Shuram excursion occurred from 585 to 579 Ma, and that incision of the Rainstorm Member shelf occurred during the 579 Ma Gaskiers glaciation. It further suggests that the base of the Johnnie Formation is ca. 630 Ma, consistent with the underlying Noonday Formation representing a Marinoan cap carbonate sequence. Our results contrast with suggestions by previous workers that the Shuram excursion followed the Gaskiers event by some 20–30 m.y. We suggest instead that the Shuram and Gaskiers events were contemporaneous with the biostratigraphic transition from acanthomorphic to leiospherid acritarchs, and with the first appearance of widespread macroscopic animal life, 38 m.y. prior to the Ediacaran-Cambrian boundary.

INTRODUCTION

Ediacaran strata record a critical period in Earth history (635–541 Ma), during which metazoan life first appeared (Knoll et al., 2004, 2006; Narbonne et al., 2012). They also record a significant rise in atmospheric and oceanic oxygen (Fike et al., 2006; Canfield et al., 2007; McFadden et al., 2008; Sahoo et al., 2012), which was a prerequisite to metabolic function in animals (Knoll and Carroll, 1999; Och and Shields-Zhou, 2012). Neoproterozoic oxygenation resulted in atmospheric oxygen levels generally interpreted as similar to those of the present day (Holland, 2006; Kump, 2008). Today, atmospheric oxygen levels are maintained by photosynthesis from land plants and marine organisms in roughly equal proportions (e.g., Field et al., 1998). It has therefore long been enigmatic that land plants are not preserved in rocks older than ca. 400 Ma, or ~150 m.y. later than the first appearance of animals. For that reason, it is widely presumed that the rise of animal life required sufficient oxygen production, from either marine photosynthesis, or perhaps some sort of "bootstrap" mechanism from animals themselves, to survive (e.g., Butterfield, 2009; Lenton et al., 2014). In any event, progress toward understanding the fundamental question, "what is the origin of animals?," hinges in part on understanding how and when oxygen became sufficiently available to make animal metabolism possible (e.g., Nursall, 1959).

Among the most fruitful avenues of research along these lines to date has been exploration of proxies for the chemistry of seawater in which animal life first appeared, primarily the stable isotope geochemistry of shallow-marine carbonate strata. The best-preserved Ediacaran strata around the globe that contain carbonate all feature a singularly large (by about a factor of two) negative anomaly in the isotopic composition of carbon, which has been attributed primarily to the isotopic composition of ancient seawater itself (Fike et al., 2006; McFadden et al., 2008; but for an alternative view, see Swart and Kennedy, 2012). The anomaly is best preserved and documented in the Ediacaran Shuram Formation in Oman (Burns and Matter, 1993; Le Guerroué et al., 2006a, 2006b; Osburn et al., 2015), and it is generally referred to as the "Shuram excursion," taking its name from the discovery formation. A similar excursion has been documented in Neoproterozoic sections on five of Earth's seven modern continents, and it occurs only once in each section: Africa (Kaufman et al., 1991; Halverson et al., 2005), Asia (Burns and Matter, 1993; Condon et al., 2005; Melezhik et al., 2005; Fike et al., 2006; McFadden et al., 2008; Macdonald et al., 2009; Osburn et al., 2015), Australia (Calver, 2000; Husson et al., 2015), Europe (Melezhik et al., 2005; Prave et al., 2009), and North America (Myrow and Kaufman, 1999; Corsetti et al., 2000; Corsetti and Kaufman, 2003; Kaufman et al., 2007; Bergmann et al., 2011; Petterson et al., 2011; Verdel et al., 2011;

Macdonald et al., 2013). The Shuram excursion is the largest known Neoproterozoic or younger carbon isotope anomaly (Grotzinger et al., 2011), and its magnitude is among the largest recorded in Earth history (see, for example, the Paleoproterozoic Lomagundi-Jatuli excursion; Bekker and Holland, 2012).

Global chemostratigraphic expression of the Shuram excursion is a remarkable discovery from at least three perspectives. First, it represents a presumably isochronous fingerprint of a specific interval of time from sections with notoriously sparse age constraints. Second, it implies that a geologically extreme event of uncertain origin occurred at the same time as the rise of animals. Last, the singular magnitude of the excursion contributes to the goal of creating a global composite time series of secular variations in marine carbon isotope ratios. In regard to the third point, the duration of the anomaly raises the potential for using the shapes of the curves, rather than simply the magnitudes of the excursions, as a correlation tool from section to section; this of course presumes a relatively constant sedimentation rate at the hundred-meter scale (Halverson et al., 2005; Saltzman and Thomas, 2012). For the Shuram excursion, $\delta^{13}C$ values rapidly descend with stratigraphic position to <–11‰, followed by a recovery that is at first gradual and then moderate in slope, with the change occurring near –4‰ (fig. 2 *in* Condon et al., 2005; fig. 3 *in* Prave et al., 2009; fig. 16 *in* Verdel et al., 2011; fig. 3 *in* Grotzinger et al., 2011; fig. 13 *in* Macdonald et al., 2013; fig. 1A *in* Husson et al., 2015).

At present, the most significant impediment to understanding Ediacaran biostratigraphy is the lack of internal age control in most sections around the globe. The ages of the boundaries of the Ediacaran Period are well defined radiometrically in multiple sections. The base is defined by the lithologically distinctive post-Marinoan cap carbonate sequence, which is associated with a –6‰ $\delta^{13}C$ excursion in carbonate and is precisely dated at 635 Ma in Namibia and China (Hoffmann et al., 2004; Condon et al., 2005). The top is defined by the first appearance of the trace fossil *Treptichnus pedum* (541 Ma), which is also associated with a –6‰ $\delta^{13}C$ excursion in carbonate. Other than the first appearance of large Ediacaran body fossils, which usually occurs rather high in most sections relative to the Ediacaran-Cambrian boundary, the Shuram excursion has emerged as the single most distinctive stratigraphic datum that is globally recognized. However, its precise age is poorly constrained, precluding any attempt to meaningfully subdivide some 94 m.y. of Ediacaran time, and creating first-order uncertainties in the relative timing of major environmental and biostratigraphic events (Xiao et al., 2016). A second major stratigraphic feature, largely restricted to sections in the North Atlantic region, is the Gaskiers glaciation (Myrow and Kaufman, 1999), which, in contrast to the Shuram event, is precisely dated at 579 Ma (Bowring et al., 2003a, 2003b; Pu et al., 2016). The mismatch between sections with glaciogenic rocks and precise radiometric ages on one hand, and the Shuram excursion in carbonate strata on the other, has left it uncertain whether or not these two events are correlative (Xiao et al., 2016). A 580 Ma age for the Shuram excursion provides an obvious correlation between the two most conspicuous events in the Ediacaran record (e.g., Xiao et al., 2004; Fike et al., 2006; Zhou et al., 2007; Halverson et al., 2005, 2010; Loyd et al., 2012; Schiffbauer et al., 2016). Alternatively, the stratigraphic proximity of the Shuram excursion to the Precambrian-Cambrian boundary, and a 551 Ma ash bed near the apparent upper zero crossing of the excursion in the Doushantuo Formation of China, suggest that it may be as much as 20–30 m.y. younger than the Gaskiers glaciation (Condon et al., 2005; Bowring et al., 2007; Cohen et al., 2009; Sawaki et al., 2010; Narbonne et al., 2012; Macdonald et al., 2013; Tahata et al., 2013; Xiao et al., 2016).

One chronological tool that has heretofore only been sparingly applied to Ediacaran strata is thermal subsidence analysis (e.g., Le Guerroué et al., 2006b). It is well known that thermal subsidence associated with seafloor spreading is a useful chronometer that can predict the age of the ocean floor based on the exponential decay of its elevation with respect to the abyssal plains for lithosphere older than 20 m.y. (e.g., equation 22 in Parsons and Sclater, 1977). The same principle also applies to models of the subsidence history of passive-margin basins, which include an initial thickness of newly stretched continental crust and substantial sediment loading (McKenzie, 1978). The decay is predicted by laws of diffusive heat transport of physical rigor that are on par with laws of closed-system radioactive decay used to date the timing of crystallization of minerals. The principal limitations in using thermal conduction as a chronometer are (1) the requirement that subsidence records thermal relaxation without significant mechanical modification of the lithosphere, such as extension, flexural loading, instability of a thermal boundary layer, or unmodeled sources of dynamic topography; and (2) corrections of the observed stratigraphic subsidence for the compaction and lithification of sediment after deposition, and for water depth and changes in sea level (e.g., Steckler and Watts, 1978; Allen and Allen, 2005).

In comparison with Phanerozoic sedimentary basins, published subsidence analyses of Ediacaran strata have been limited, with most of the effort thus far concentrated on the western Laurentian continental margin (Stewart and Suczek, 1977; Bond et al., 1983; Armin and Mayer, 1983; Levy and Christie-Blick, 1991; Yonkee et al., 2014). The focus on this region as a testing ground for thermal subsidence modeling was due to the fact that it is perhaps the best-preserved example of an ancient passive margin, analogous to present-day Atlantic-type margins, but with virtually complete surface exposure of apparent synrift and postrift sedimentary archives spanning several hundred million years (Stewart, 1972; Gabrielse, 1972; Burchfiel and Davis, 1972, 1975; Stewart and Poole, 1974; Dickinson, 1977; Monger and Price, 1979). Because these sequences span the Ediacaran-Cambrian boundary, such that roughly half their thickness is Proterozoic in age, temporal control on subsidence has been restricted mainly to the Phanerozoic portion of subsidence curves. The lack of age control on the lower part of the section precludes precise definition of the transition from mechanical extension to pure thermal subsidence. Fortunately, the accurate definition of an exponentially decaying system, in particular, extrapolating stratigraphic age backward in time from a curve with known ages, is independent of the timing of onset and total amount of purely thermal subsidence.

Here, we address the problem of the correlation and age of the Shuram isotopic excursion through lithostratigraphic and chemostratigraphic study of the type locality of the Ediacaran Johnnie Formation in the Spring Mountains of southern Nevada. The Johnnie Formation is at least 1800 m thick at the type locality, and it makes up more than half of the maximum known thickness of ~3000 m of total Ediacaran strata exposed in this region. The underlying Noonday Formation provided the first isotopic match between the Marinoan cap carbonate sequence in Namibia (Hoffman et al., 1998) and a section from another continent (Petterson et al., 2011). The overlying Stirling and Wood Canyon Formations contain Ediacaran and Lower Cambrian fossil assemblages that define the Cambrian-Precambrian boundary within the lower part of the Wood Canyon Formation (Corsetti and Hagadorn, 2000; Hagadorn and Waggoner, 2000), 1200 m above the top of the Johnnie Formation in the Spring Mountains. The uppermost 300 m of section of the Johnnie Formation contains the best expression of the Shuram excursion in Laurentia (Corsetti and Kaufman, 2003; Kaufman et al., 2007; Bergmann et al., 2011; Verdel et al., 2011). Therefore, to the extent that the section was deposited at or very near sea level on a thermally subsiding continental shelf, subsidence analysis may be used to estimate the age of the Shuram excursion and perhaps even broadly constrain the overall age of the Johnnie Formation.

GEOLOGIC SETTING

Neoproterozoic–Cambrian strata in western Laurentia are divisible into two principal components, including a lower diamictite and volcanic sequence, and an upper terrigenous detrital sequence (Stewart and Suczek, 1977; Poole et al., 1992). The Johnnie Formation is the lowest siliciclastic formation in the upper terrigenous detrital sequence, forming the basal deposits of a westward-thickening continental margin terrace wedge, widely regarded to have developed in the wake of late Neoproterozoic rifting of the Rodinian supercontinent (Li et al., 2008, 2013). The formation is a few hundred meters thick near its eastern pinchout beneath Lower Cambrian cratonic strata, systematically increasing to at least 1500 m thick in its westernmost exposures, where the base is not definitively exposed (Stewart, 1970; this report). Lithologically, it is primarily variegated siltstone and very fine-grained sandstone that contains varying amounts (10%–40%) of carbonate and orthoquartzite, distinguishing it from the carbonate-dominated Noonday Formation below and coarse siliciclastic rocks of the Stirling Formation above (Fig. 1).

The Johnnie Formation was first defined and described in the northwest Spring Mountains in the Johnnie Wash area (Fig. 2; Nolan, 1924, 1929), where its contact with the underlying Noonday Formation is apparently not exposed, and hence its thickness is a minimum for this location. Nolan's (1924) thickness and description were included in the regional stratigraphic synthesis of Stewart (1970). The type locality was subsequently mapped and briefly described by Burchfiel (1964, 1965), and relatively complete lithostratigraphic sections were measured by Hamill (1966) and Benmore (1978). The type locality has since received little attention in comparison to the much thinner sections in the Nopah Range and environs 70 km to the south, or equivalents 100 km to the west in the Panamint Range, where its basal contact with the Noonday Formation is extensively exposed (e.g., Hazzard, 1937; Wright and Troxel, 1966; Labotka et al., 1980; Albee et al., 1981; Benmore, 1978; Summa, 1993; Fedo and Cooper, 2001; Corsetti and Kaufman, 2003; Kaufman et al., 2007; Verdel et al., 2011). With the exceptions of detailed studies of parts of the formation (Summa, 1993; Abolins, 1999; Bergmann et al., 2011), no systematic attempt has yet been made to describe and interpret the entire formation at its type locality in terms of key bed forms, depositional environments, sequence architecture, or chemostratigraphy, at the level of more southerly or westerly sections.

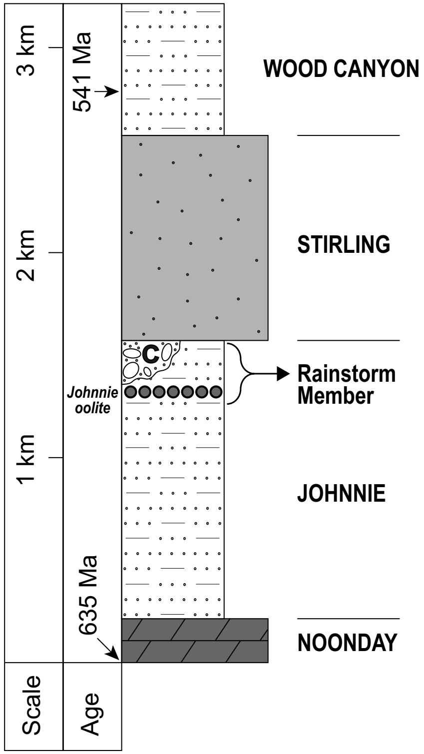

Figure 1. Generalized stratigraphic column of Precambrian–Cambrian strata; thicknesses represent sections in the northwest Spring Mountains, Nevada (from Stewart, 1970). Cryogenian-Ediacaran boundary (635 Ma) is based on the interpretation that the Noonday Dolomite is the Marinoan cap carbonate sequence (Petterson et al., 2011) and the definition for the base of the Ediacaran Period (Knoll et al., 2004, 2006; Narbonne et al., 2012). Precambrian-Cambrian boundary (541 Ma) is based on paleontology (Hagadorn and Waggoner, 2000; Corsetti and Hagadorn, 2000). The Noonday Formation and Stirling Formation are generally resistant, cliff-forming units, in contrast to the recessive, slope-forming Johnnie and lower Wood Canyon formations. The letter C indicates the conglomeratic member of the Johnnie Formation, which fills local valleys incised into the Rainstorm Member.

The uppermost part of the Johnnie Formation, the Rainstorm Member, is a lithostratigraphically distinctive unit that can be correlated with confidence over a broad region of southwestern North America, including eastern California and southern Nevada (Stewart, 1970), and it probably occurs as far south as northern Sonora, Mexico, where it forms a part of the Clemente Formation (Stewart et al., 1984). The basal strata of the Rainstorm Member are its most distinctive part. They include a thin (~2 m), siltstone-enveloped, regionally extensive oolitic marker bed known as the "Johnnie oolite" (e.g., Bergmann et al., 2011). The oolite is underlain by greenish gray siltstone, and it is over-

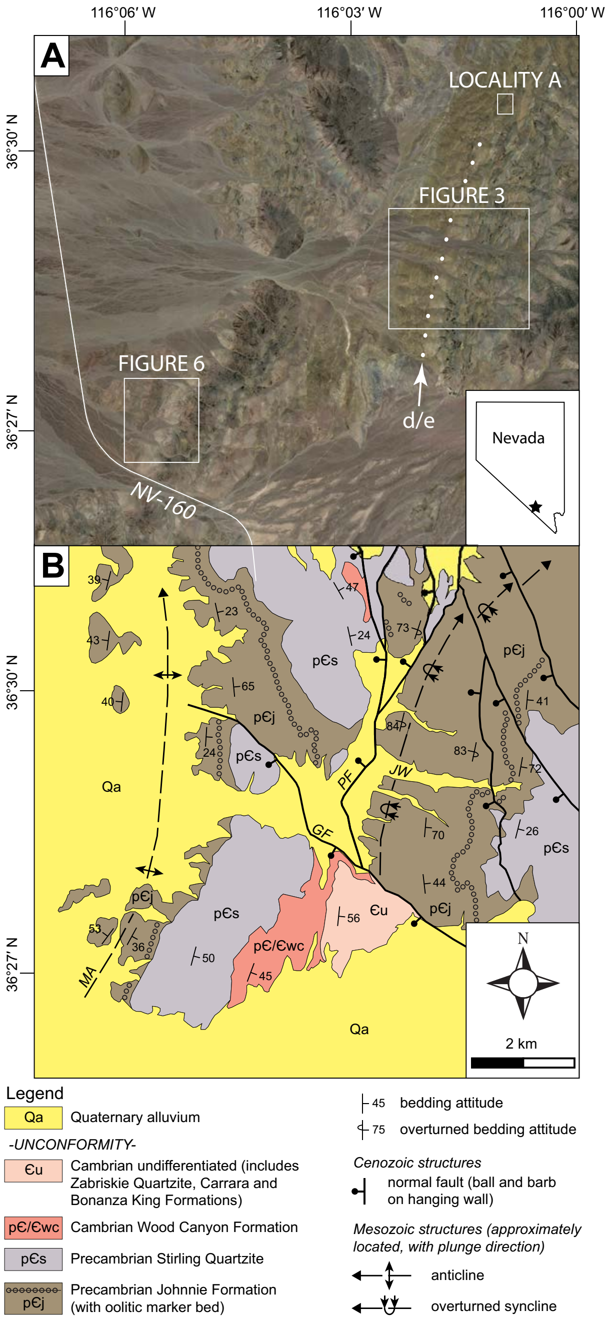

Figure 2. (A) Google Earth image and (B) corresponding geologic map of Precambrian–Cambrian strata in the northwest Spring Mountains, Nevada, in the vicinity of the type locality of the Johnnie Formation in Johnnie Wash. GF—Grapevine fault; JW—Johnnie Wash; MA—Montgomery anticline; NV-160—Nevada State Highway 160; PF—Paddy's fault. Dotted line labeled d/e indicates the conspicuous surface trace of the contact between informal members D and E of the Johnnie Formation. Data were compiled from Abolins (1999), Burchfiel et al. (1974, 1983), and this study.

lain by distinctive pale-red, fine-grained sandstone with or without associated sandy or silty micrites ("liver-colored limestones"). The overlying units characteristically contain groove marks, flute casts, intraformational conglomerate, and other indicators of shallow-water, high-energy currents. These carbonates record the onset and most negative part of the Shuram excursion in eastern California and southern Nevada (Corsetti and Kaufman, 2003; Kaufman et al., 2007; Verdel et al., 2011), as well as in the Sonora sections (Loyd et al., 2012). Similar to formation-scale thickness variations in the terrigenous detrital sequence as a whole, the Rainstorm Member generally thickens westward from as little as 20 m in the thinnest measured section to more than 300 m in the thickest sections (Stewart, 1970; Verdel et al., 2011).

Lower and middle Johnnie Formation strata are sufficiently variable in their lithostratigraphy that recognition of regionally mappable members is not as straightforward as in the case of the Rainstorm Member. As noted by Summa (1993), sub–Rainstorm Member depositional settings of the Johnnie Formation are interpreted as inner-shelf to tidally influenced nearshore environments that were highly susceptible to sea-level fluctuation (Benmore, 1978; Fedo and Cooper, 2001; Schoenborn et al., 2012). As we describe herein, depositional environments tend to be more landward to the south and east in these units, as suggested by the abundance versus absence of desiccation features, fluvial versus marine deposition, and medium- to coarse-grained sandstones versus fine- to medium-grained sandstones. Although this variability complicates simple lithostratigraphic correlation, if interpreted correctly, it can be used as an effective indicator of sea-level rise and fall.

Reported age constraints from the Johnnie and correlative Clemente formations include (1) a 640 Ma U-Pb age from a single detrital zircon grain in sub–Rainstorm Member siltstones in the Panamint Range of eastern California (Verdel et al., 2011), and (2) potential Ediacaran body and trace fossils (e.g., *Cyclomedusa plana* and *Palaeophycus tubularis*, respectively) ~75 m below the oolite in the Clemente Formation (McMenamin, 1996). The U-Pb age, because it is based on a single grain, is subject to the uncertainty of contamination during mineral processing and needs to be confirmed with duplicate analyses. The putative fossils have been questioned after examination by other paleontologists (e.g., J.W. Hagadorn, 2017, personal commun.), and they have generally not been accepted in subsequent stratigraphic studies of the region (e.g., Loyd et al., 2012, 2015). Latest Ediacaran fossils have been recovered from the uppermost Stirling Formation and the Lower Member of the Wood Canyon Formation in the Spring Mountains and neighboring Montgomery Mountains to the south (e.g., *Cloudina* and *Swartpuntia*; Hagadorn and Waggoner, 2000; Smith et al., 2017), from sections in stratigraphic continuity with the type Johnnie Formation. These are succeeded immediately upward by Lower Cambrian trace fossils (*Treptichnus pedum*), which places the Ediacaran-Cambrian boundary in the Lower Member of the Wood Canyon Formation (Fig. 1; Corsetti and Hagadorn, 2000).

The underlying Noonday Formation has been interpreted as the cap carbonate sequence of the Marinoan "snowball Earth" glaciation (Petterson et al., 2011), which by definition would place its base at the beginning of the Edia-

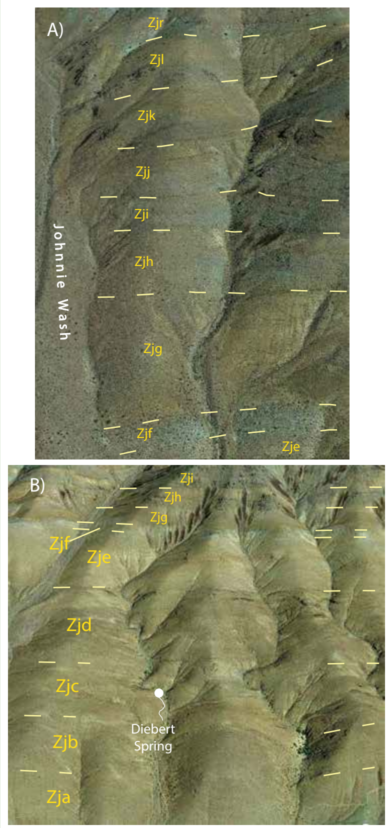

caran period (635 Ma; Knoll et al., 2004, 2006; Narbonne et al., 2012). The Johnnie Formation's basal contact with the Noonday Formation is lithostratigraphically gradational, transitioning from sandy dolostones of the upper Noonday Formation (Mahogany Flats Member of Petterson et al., 2011) to interstratified dolomitic sandstone and orthoquartzite in the lower Johnnie Formation (Transitional Member of Stewart, 1970). Although traditionally regarded as a conformable contact on the basis of this gradation (Hazzard, 1937; Stewart, 1970; Wright and Troxel, 1984), the identification of local karstic surfaces along the contact raises the possibility that it is a disconformity with a substantial depositional hiatus (Summa, 1993).

In terms of chemostratigraphic constraints on age, the conspicuous excursions to –6‰ at the base and top of the Ediacaran section are well expressed in the south Laurentian sections (e.g., Petterson et al., 2011; Smith et al., 2016). The presence of the Shuram excursion in the Rainstorm Member, despite its value as a correlation tool, does little to constrain the depositional age, because unlike the tightly constrained boundary excursions, hard chronological constraints are lacking, as noted already.

For almost a century, the terrigenous detrital sequence has been studied extensively on many different levels. Much of the early work focused on stratigraphic group-level packages that record the transition from Precambrian to Cambrian time (Nolan, 1929; Burchfiel, 1964; Stewart, 1970). More recent work on the Johnnie Formation has focused largely on outcrops in eastern California (Summa, 1993; Fedo and Cooper, 2001; Verdel et al., 2011; Schoenborn and Fedo, 2011; Schoenborn et al., 2012), or on specific features related to the Rainstorm Member, such as an incision-related conglomeratic member (Summa, 1993; Abolins, 1999; Abolins et al., 2000; Clapham and Corsetti, 2005; Verdel et al., 2011), giant ooids (Trower and Grotzinger, 2010), or detailed chemostratigraphy of the Johnnie oolite (Bergmann et al., 2011). The lower and middle portions of the Johnnie Formation have not been given as much detailed attention, except in areas close to the craton miogeoclinal hinge, where the Johnnie Formation is only a few hundred meters thick. The 1600 m stratigraphic thickness of sub–Shuram excursion Johnnie Formation at the type locality exceeds the thickness of any globally correlative Ediacaran strata of which we are aware. Furthermore, total Ediacaran stratigraphic thickness in southwest Laurentia measures over 3000 m, greater than the approximate thicknesses of sections in Australia (2500 m), Oman (1500 m), and China (300 m). Strata of the lower and middle Johnnie Formation at its type locality therefore represent one of the best opportunities among sections globally to provide a relatively complete record of Ediacaran time prior to the Shuram excursion. An important gap in our understanding of Ediacaran chemostratigraphy is the paucity of carbonate strata below the Shuram anomaly in most sections. Of the major global sections that contain it, only the Oman example contains abundant carbonate in immediately underlying strata, the Khufai Formation. Discovery of correlative carbonate-bearing strata in one or more sections around the globe would thus represent a significant step in expanding the global inventory of chemostratigraphic time series for a critical interval in Neoproterozoic time.

METHODS

Lithostratigraphy

To identify a structurally intact section of the Johnnie Formation, we performed geologic mapping at 1:10,000 scale in the northwest Spring Mountains, Nevada, both of the type locality at Johnnie Wash, and in an area ~4 km to the southwest near Nevada Highway 160, 3 km west-southwest of Mount Schader (Fig. 2). We used the Mount Schader, Nevada 1:24,000 quadrangle map (U.S. Geological Survey, 1968) as a topographic base. Our field mapping spanned 9 d total between 21 April 2015 and 2 May 2015. The geologic maps were used to identify optimum transects for measuring stratigraphic section. The Mount Schader section was measured and sampled in detail using a Jacobs staff mounted with a Brunton® compass set to the dip of bedding. For each stratigraphic subunit, we recorded: (1) fresh and weathered color of lithology using a Munsell color chart; (2) grain size; and (3) bedding thickness (supplemental text[1]). Section was measured to the resolution of ~0.5 m (or finer in some instances, if warranted). The Johnnie Wash section was measured using geologic cross sections, and the general lithologic characteristics were recorded in the field during geologic mapping (see Appendix for unit names and descriptions).

Chemostratigraphy

For carbon and oxygen isotope chemostratigraphy, we collected samples at 0.3–1 m resolution in carbonate units. Samples from the upper ~400 m of sub–Rainstorm Member lithostratigraphic units were collected from the Mount Schader section during stratigraphic logging. Samples from two prominent carbonate horizons that occur below the deepest exposed strata of the Mount Schader section were collected in the Johnnie Wash locality of the Spring Mountains, and at a location ~3 km north of Johnnie Wash (locality A in Fig. 2A). In total, 107 centimeter-scale sample chips were collected for carbon and oxygen isotopic analysis, including 36 from the Johnnie Wash section and locality A and 71 from the Mount Schader section. In the laboratory, sample chips were sliced open using a diamond-bladed wet saw to expose fresh, unweathered surfaces. From the fresh surfaces, a high-speed rotary tool with a diamond-tipped drill bit was used to powder the sample. We carefully extracted ~0.1 mg of analyte from each sample chip, taking care to avoid any visible alteration or veining. Sample powder was loaded into vials, the air was purged and replaced with helium gas, and then digested in phosphoric acid at 72 °C for at least 1 h to evolve sufficient CO_2 gas for analysis. Carbon and oxygen isotope ratios were measured at Caltech using a Delta V Plus isotope ratio mass spectrometer ("gas bench"). Our values for $\delta^{13}C$ and $\delta^{18}O$ are reported relative to the Vienna Peedee belemnite (VPDB) standard in per mil notation. We used Caltech's laboratory working standards, which were calibrated to NBS 18 and NBS 19 and have uncertainties of ±0.1‰. Standards were measured once for every nine samples to assess systematic error.

[1]Supplemental Items. Six figures (Figures S1–S6), two tables (Tables S1 and S2), and supplemental text. Please visit https://doi.org/10.1130/GES01678.S1 or access the full-text article on www.gsapubs.org to view the Supplemental Items.

Subsidence Analysis

Our tectonic subsidence analysis is based on stratigraphic thicknesses compiled from multiple sources for the northwest Spring Mountains, Nevada. The inner-shelf to fluvial-deltaic facies of virtually all units within the terrigenous detrital sequence in this region suggest shallow-water deposition, removing the need for paleobathymetric correction (Levy and Christie-Blick, 1991). We used thicknesses from this study combined with thicknesses for overlying formations principally based on Stewart (1970) and Burchfiel et al. (1974). Our analysis encompasses known time points ranging from the Ediacaran-Cambrian boundary in the Lower Member of the Wood Canyon Formation (Corsetti and Hagadorn, 2000; Hagadorn and Waggoner, 2000; Smith et al., 2016, 2017) at 541 Ma, up through the Devonian-Mississippian boundary at the top of the Devils Gate Formation (Burchfiel et al., 1974) at 359 Ma (Ogg et al., 2016). The only previous attempt at a geohistory analysis of the Spring Mountains (Levy and Christie-Blick, 1991) was temporally constrained mainly by the Lower-Middle and Middle-Upper Cambrian boundaries, which were then deemed to be ~30 m.y. older than their currently accepted ages. We followed methods described in Allen and Allen (2005) to delithify and progressively unload (backstrip) the stratigraphic column in order to obtain the tectonic component of subsidence. Delithification parameters for siliciclastic rocks were taken from table 9.1 *in* Allen and Allen (2005), and parameters for carbonate rocks were taken from Equation 3 *in* Halley and Schmoker (1983). Tectonic subsidence curves were calculated using Backstrip, an open-source software for decompaction and tectonic subsidence calculations (Cardozo, 2009). Results for our earliest model runs were verified by hand using a spreadsheet program (e.g., Larrieu, 1995).

RESULTS

Lithostratigraphy

The most salient feature of the Johnnie Formation in the Johnnie Wash type locality (Fig. 3) is that, although very fine-grained sandstone and siltstone are present in all mappable units (distinguishing it from the overlying Stirling and underlying Noonday formations), three intervals are characterized by an abundance of fine- to medium-grained sandstone (identified with Roman numerals I, II, and III on Fig. 4). The sand-rich intervals range from 160 to 430 m thick, form distinct, resistant ridges within the otherwise recessive Johnnie Formation, and establish a basis for subdividing it into mappable units. Each sand-rich interval exhibits characteristics that readily distinguish it from the other two, in terms of either bed forms (intervals I and II) or parasequence architecture (interval III). Further subdivision of the formation is afforded by a conspicuous, 30–40-m-thick cherty carbonate unit near the middle of the section, and by lithological variation within sand-rich interval III. Our subdivision into map units includes the Rainstorm Member at the top, underlain by 12 informal units designated A through L (Fig. 4; Fig. S1 [footnote 1]). Sand-rich intervals I and II define units B and D, and their enveloping sand-poor strata define units A, C, and E. The cherty carbonate marker and overlying sand-poor strata define units F and G. The upper sand-rich interval exhibits rhythmic variations of sandstone, siltstone, and carbonate that are divided into five units, H through L, each of which is defined at the base of a 30–100-m-thick sand-rich subinterval (Figs. 3 and 4; Fig. S1 [footnote 1]).

At the Johnnie Wash type section, bedding strikes approximately north-south and dips moderately to steeply eastward (Fig. 3). The total thickness of sub–Rainstorm Member strata is 1595 m. The lowest stratigraphic unit (unit A) encountered is a recessive, slope-forming phyllitic siltstone that contains a continuous cleavage at high angle to bedding. The base of unit B is defined by the lowest occurrence of meter-scale orthoquartzite beds, which are abundant in the unit. Unit B is readily distinguished from higher sand-rich intervals by pervasive penecontemporaneous deformation. Nearly every sandstone horizon is affected, principally by ball-and-pillow structure, so much so that individual orthoquartzite beds are difficult to trace along strike for more than a few tens of meters. Individual ball-and-pillow structures are up to meter-scale in size (roughly equal to orthoquartzite bed thickness) and occur where fine-grained sandstone and siltstone underlie coarser sandstone. The ball-and-pillow structure is manifested in some places as simple load casts with folded lamination (Fig. 5A) and in others as completely detached sand bodies that have slumped downward into the underlying siltstone, surrounded by flame structure developed within the siltstone (Fig. 5B). At the type locality, the occurrence of ball-and-pillow structure in the Johnnie Formation is restricted to unit B, but it was also observed along one horizon at the top of the Rainstorm Member in the Mount Schader section (Figs. 6 and 7).

Unit C marks a return to generally inconspicuous, slope-forming siltstone with a prominent orthoquartzite marker horizon near the middle of the unit. The uppermost beds include a brown, resistant, 2-m-thick dolostone bed, which marks the lowest occurrence of carbonate in the type section.

Unit D includes orthoquartzite and less abundant siltstone. The sedimentary characteristic that distinguishes unit D from the other two sand-rich intervals is abundant high-angle cross-stratification, preserved in medium- to thick-bedded orthoquartzite (Fig. 8A). Millimeter- to centimeter-scale laminae or thin beds are preserved in foresets within decimeter- to meter-scale beds that can be followed for tens of meters along strike. Foreset lamination is consistently truncated at high angles, ranging from 20° to 30°, by overlying beds (Fig. 8B). In stratigraphic coordinates (corrected by tilting to horizontal about the line of strike), poles to foreset lamination are strongly unimodal, dispersed in trend by more than 90° around a mean vector of ~N30°E 65° (Fig. 8B). We measured grain-size variation with stratigraphic height across a sequence of about 10 foreset layers (Figs. 8C and 8D) to test for the presence of reverse grading, which is characteristic of dry grain flows on the lee side of dunes (e.g., Hunter, 1977; Boggs, 2012). The results indicated that the mean grain size of ~200 μm varies little through the sample, if anything fining slightly upward. In general, the lamination is not defined by concentrations of detrital heavy minerals. Opaque phases in these quartzites are largely diagenetic and relatively uniformly distributed throughout the rock.

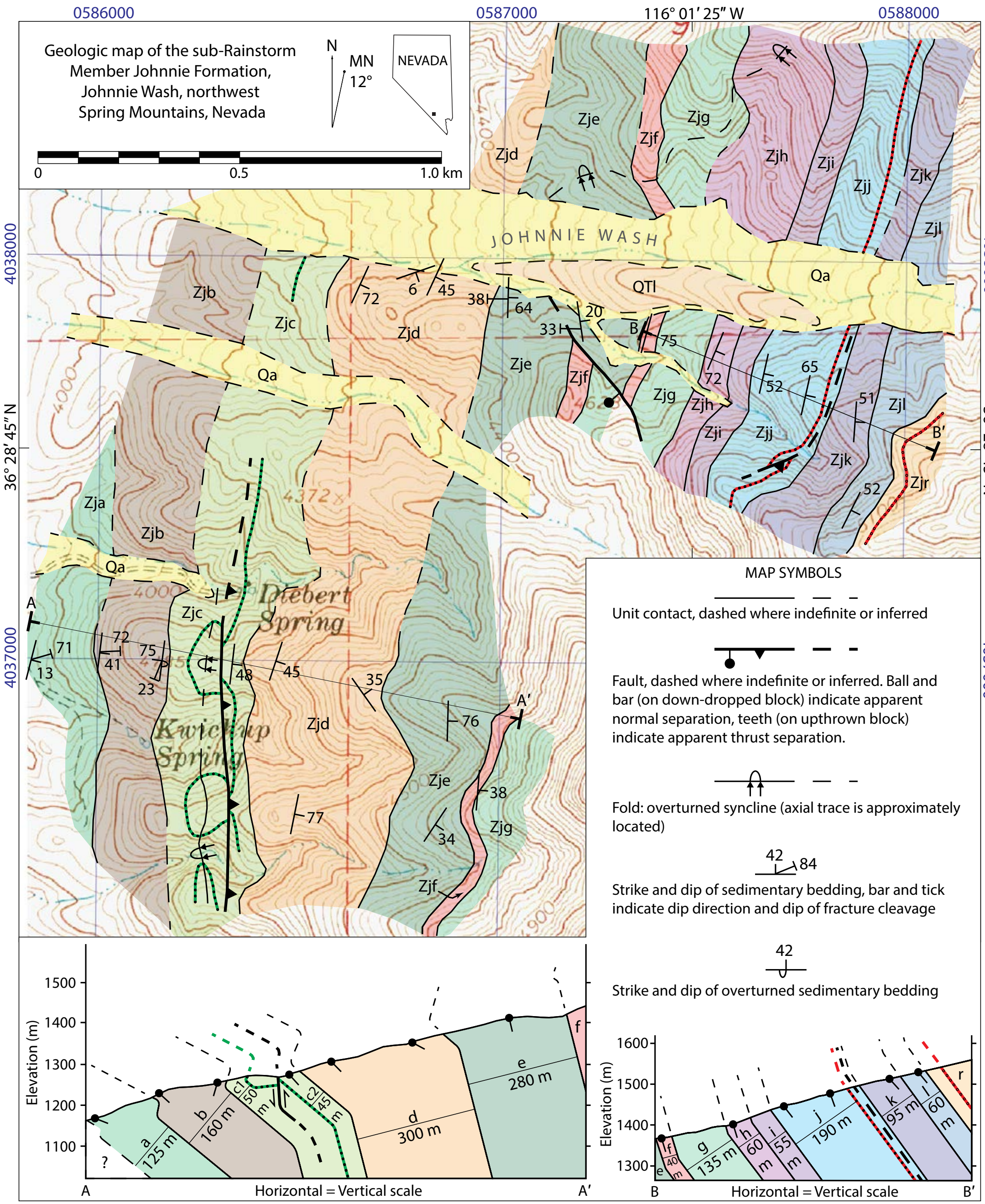

Figure 3. Geologic map and cross sections of Johnnie Wash and environs. Definitions of unit labels and description of map units are given in the Appendix.

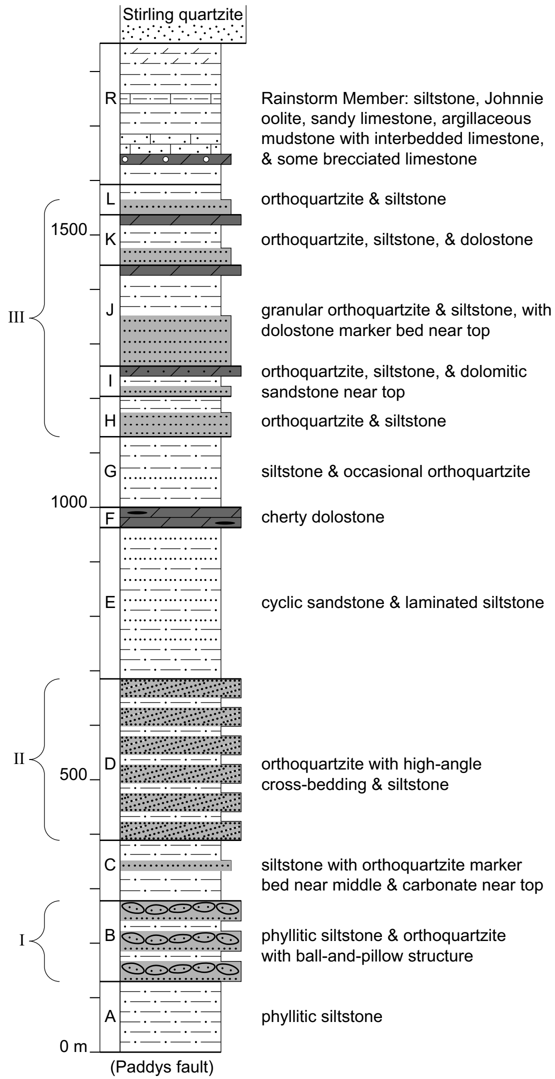

Figure 4. Generalized lithostratigraphic column of the Johnnie Formation at its type locality in Johnnie Wash, with thicknesses based on cross sections A-A′ and B-B′ in Figure 3 for units A through L, and Stewart (1970) for the Rainstorm Member. Roman numerals on left side of column indicate the three sand-rich intervals discussed in text.

The boundary between units D and E is among the most readily mappable in the area and is also associated with a color change on remote imagery from dark brown to light brown, which is the most conspicuous color contrast in the section (Fig. 2A). Unit E is ~280 m thick, and it is dominated by very fine-grained sandstone and siltstone, generally lacking the mature, fine- to medium-grained quartzitic sandstone characteristic of unit D. Near the top, unit E contains an interval of ~30 medium-bedded cycles that alternate between massive, immature fine-grained sandstone and laminated siltstone. Unit F is a conspicuous, 30–40-m-thick, gray cherty dolostone (Fig. 5C) that can be followed for at least 5 km along strike, albeit with some minor faulting. Unit G is 135 m thick, and it returns to siltstone and very fine-grained sandstone similar to unit E, with a few inconspicuous orthoquartzite beds.

The overall lithostratigraphic character changes beginning at the base of unit H, from relatively thick, homogeneous sandstone-, siltstone-, or carbonate-dominated units below to the far more compositionally heterogeneous units above. From the base of unit H up to the base of the Rainstorm Member, the section contains abundant orthoquartzite, defining the uppermost of the three sand-rich intervals in the Johnnie Formation (Fig. 4). For mapping purposes, the most straightforward subdivision of sand-rich interval III in the Johnnie Wash area is defined by five quartzite-dominated subunits ranging from 10 to 100 m thick, which define the lower parts of units H, I, J, K, and L (Fig. 4; Fig. S1 [footnote 1]). Each of these subunits is overlain by variable thicknesses of recessive, variegated siltstone (Fig. 5E). The occurrence of carbonate is sporadic. In the section in Johnnie Wash, units I, J, and K are each capped by a resistant, 1–3-m-thick subunit of brown-weathering, laminated dolostone (Fig. 5D), and units H and L do not contain carbonate (Fig. 4). The Mount Schader section contains a lesser proportion of quartzitic sandstone and a greater proportion of carbonate and siltstone (Figs. 6 and 7), which is the basis for selecting it, instead of the type locality, for detailed measurement and chemostratigraphic sampling. Even within the Johnnie Wash area, the distribution of quartzite, siltstone, and carbonate changes along strike, on a scale of a few kilometers (Abolins, 1999). Although orthoquartzite beds in units H through L locally exhibit some high-angle cross-stratification in the Johnnie Wash section, they contrast with unit D (sand-rich interval II) in mainly being parallel-bedded or, in the case of the Mount Schader section, hummocky cross-stratified. Orthoquartzite in units H–L is generally fine- to medium-grained and appears to contrast with lower sand-rich intervals in containing a greater proportion of medium-grained and locally coarse-grained sand.

Our informal unit nomenclature ends at the base of the formally defined Rainstorm Member, which, as noted earlier, is readily identified throughout the region on the basis of lithologic characteristics. In the northern Spring Mountains, the Rainstorm Member contrasts with the underlying units H through L in lacking fine- to medium-grained orthoquartzite beds. At the base of the Rainstorm Member, a fissile, phyllitic siltstone is overlain by the ocher-colored, 2-m-thick Johnnie oolite. The ooids are up to ~2 mm in diameter (Fig. 5F) and exhibit local cross-stratification. The oolite horizon has erosional basal and upper contacts, locally including intraformational breccia and conglomerate, which includes cobbles and small boulders of the oolite. Above the Johnnie oolite, pale-red limestones locally contain dispersed, coarse quartz grains interstratified with carbonate-cemented, fine-grained sandstone. These carbonate-rich rocks are overlain by argillaceous mudstone with interbedded limestones, with scattered horizons of intraformational conglomerate.

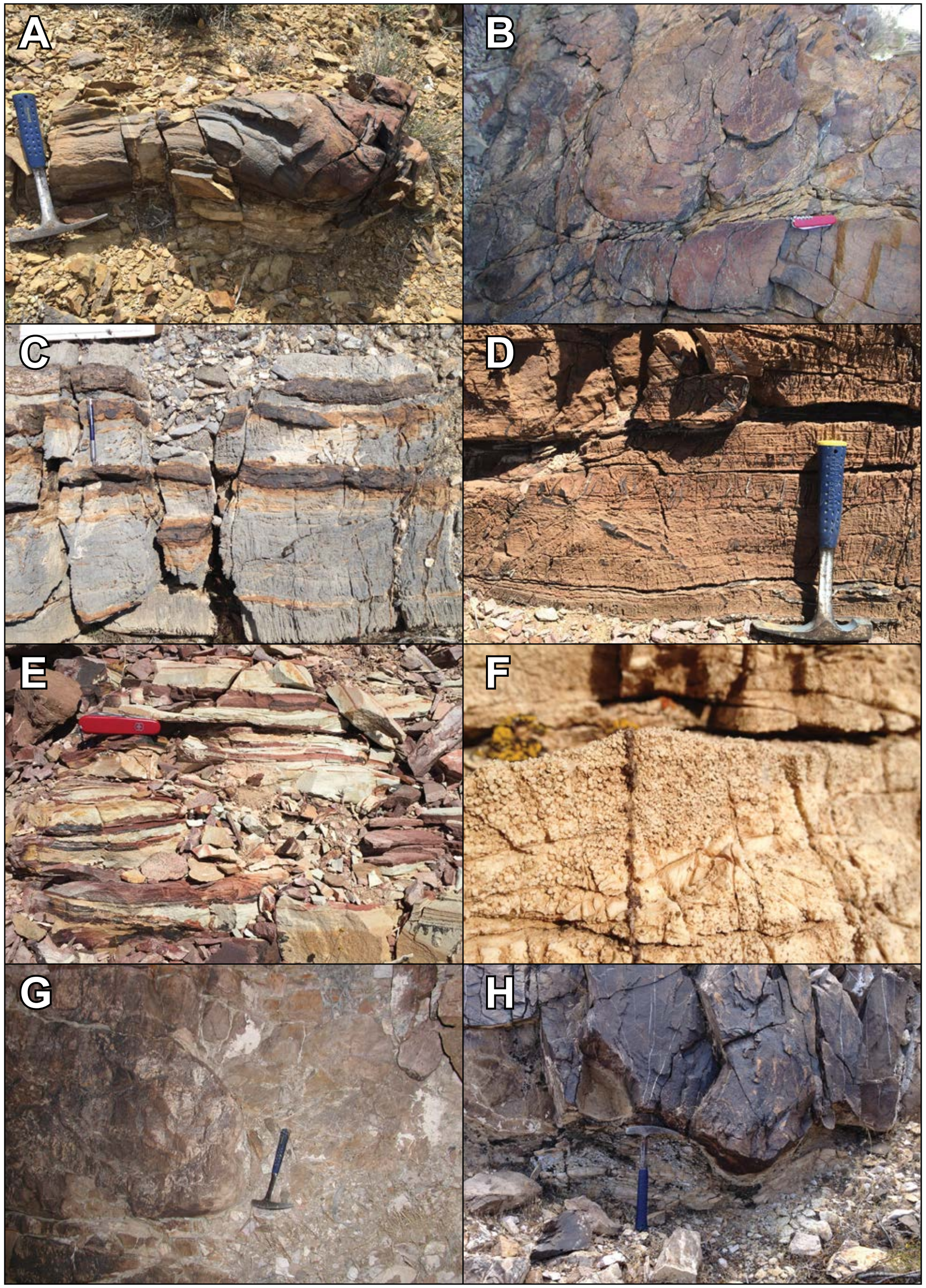

Figure 5. Photographs of selected lithostratigraphic elements of the Johnnie Formation. (A) Load cast with folded laminae in sandstone bed, unit B, Johnnie Wash area. Hammer is 28 cm long. (B) Ball-and-pillow structure in unit B, with light-colored siltstone (just above pocket knife) protruding upward between bulbous masses of fine-grained sandstone. Pocket knife is 9 cm long. (C) Gray cherty dolostone, unit F, Johnnie Wash. Pencil is 15 cm long. (D) Brown-weathering, laminated dolostone, typical of carbonate beds in units H through L. Hammer is 28 cm long. (E) Variegated siltstone typical of all units in the Johnnie Formation. Pocket knife is 9 cm long. (F) Johnnie oolite, Johnnie Wash, ooids are 1–2 mm in diameter. (G) Large, bulbous mass of orthoquartzite (left of hammer), surrounded by smaller masses lying in a matrix of siltstone, uppermost bed of the Rainstorm Member, Mount Schader section. Hammer is 33 cm long. (H) Base of orthoquartzite bed in G, showing load cast structures with underlying siltstone. Hammer is 33 cm long.

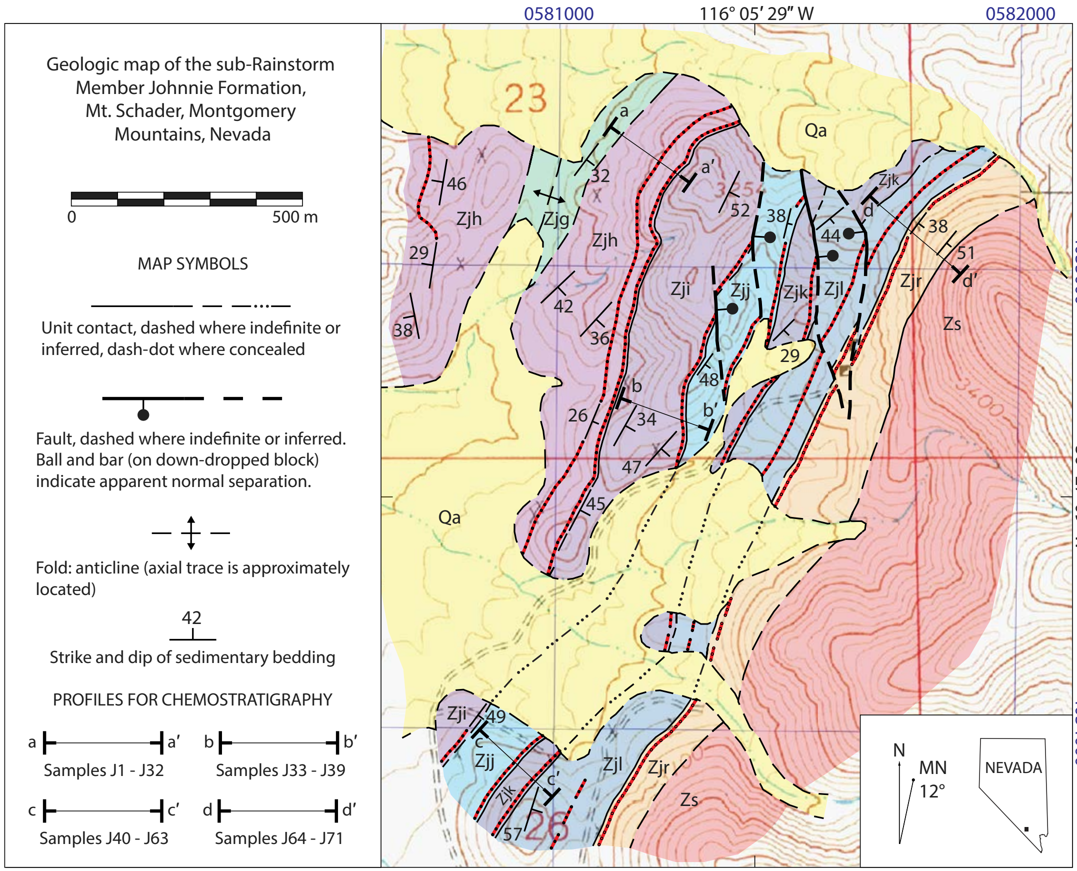

Figure 6. Geologic map of the Mount Schader section, showing measured and sampled transects. Definitions of unit labels and description of map units are given in the Appendix.

The uppermost part of the Rainstorm Member in the Mount Schader section contains a 4-m-thick triad of quartzite, siltstone, and dolostone, in which the quartzite is disrupted by locally intense ball-and-pillow structure (Figs. 5G and 5H). The base of the overlying A Member of the Stirling Formation is marked by highly resistant, massively textured to cross-stratified, medium- to thick-bedded, medium- to coarse-grained orthoquartzite. The principal contrast between the Stirling Formation's A Member and any of the orthoquartzites in the Johnnie Formation is the coarse grain size, including the common occurrence of granules and small pebbles of vein quartz and jasper. Neither the Johnnie Wash section nor the Mount Schader section appears to preserve the incised valley fill characteristic of the conglomeratic member of the Johnnie Formation (Abolins, 1999; Verdel et al., 2011).

Chemostratigraphy

Carbon isotope ratios range from a low of –4.4‰ (VPDB) to a high of 4.9‰ (Table S1 [footnote 1]). The data are mainly concentrated in carbonate beds in units H through L, which constitute the uppermost 400 m of pre–Rainstorm Member strata (Fig. 7). Within the underlying ~1100 m of exposed Johnnie Formation strata, carbonate intervals are present only in units C and F, 1440 m and 860 m below the base of the Rainstorm Member, respectively (Figs. 4 and 9). The lowest and highest values of $\delta^{13}C$ occur in the stratigraphically highest samples, and they define a strong negative trend, beginning near the top of unit K and ending at the top of the Johnnie oolite bed. Below this marked trend in the data, there is otherwise no general trend.

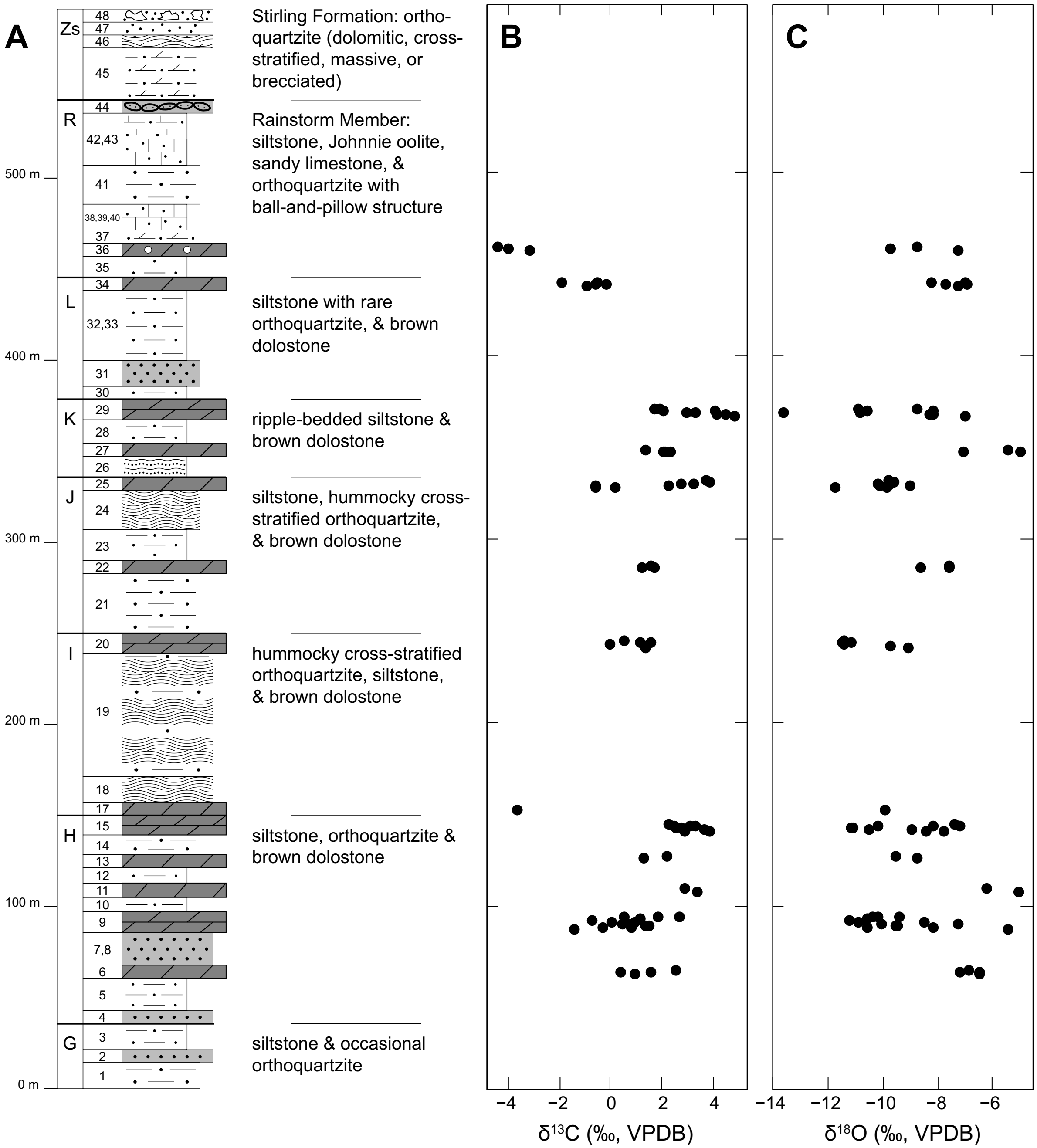

Figure 7. (A) Detailed lithostratigraphic column of the Mount Schader section, from unit G of the Johnnie Formation through the lowermost part of the A Member of the Stirling Formation, showing thicknesses based on Jacobs staff measurements (transects shown in Fig. 6). Detailed descriptions of subunits 1–48 are given in the supplemental text (text footnote 1). (B) Carbon and (C) oxygen isotope ratios in carbonate, as a function of stratigraphic position. Numerical values are in Table S1 (text footnote 1). VPDB—Vienna Peedee belemnite.

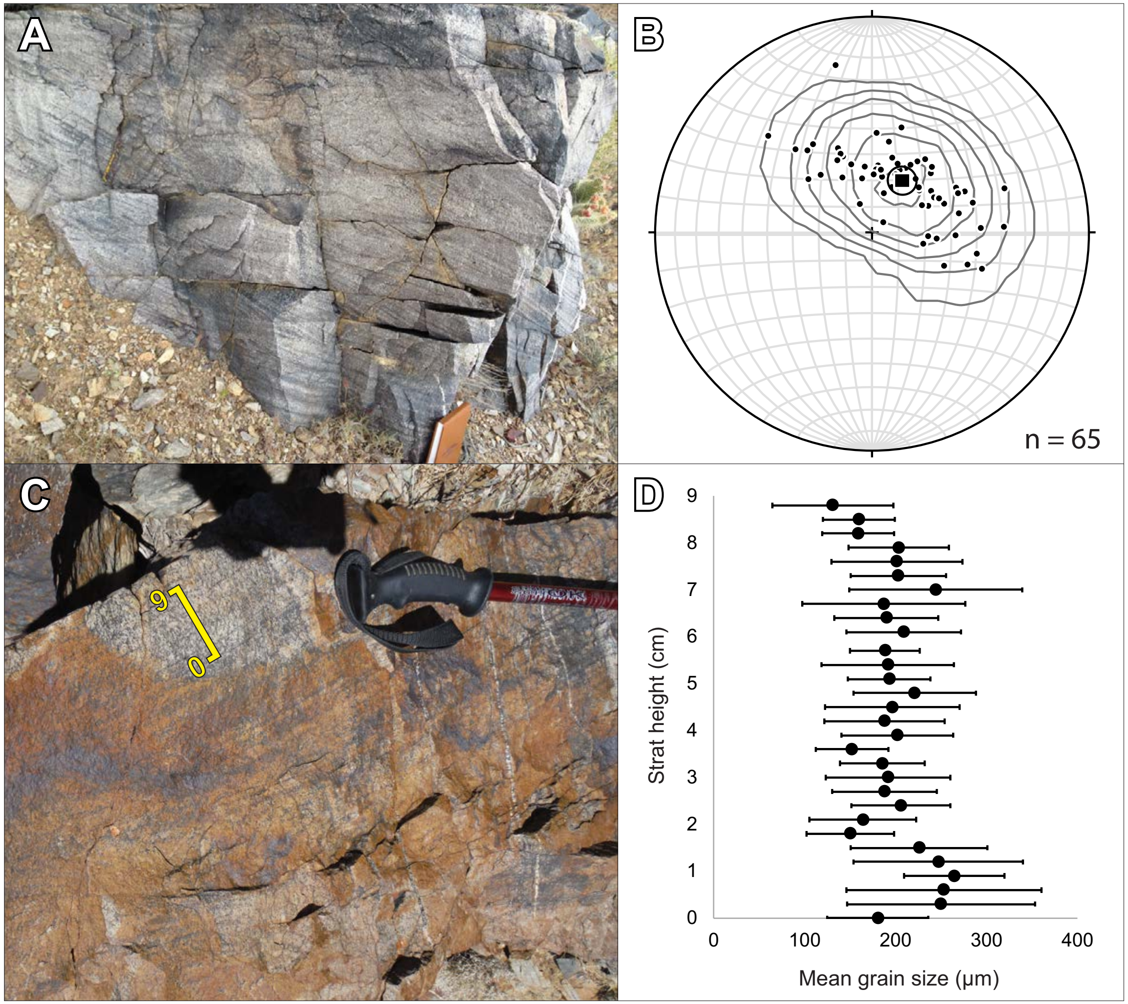

Figure 8. (A) Photograph of tabular planar cross-stratification in unit D, Johnnie Wash. Notebook is 13 cm wide. (B) Equal-area stereogram of poles to foreset laminations measured at locality A (Fig. 2A), with bedding tilt removed. Dots are data (*n* = 65); larger square in circle is the mean vector. Plotted using Stereonet software (Allmendinger et al., 2012; Cardozo and Allmendinger, 2013), with Kamb contours at 2σ intervals (Kamb, 1959). (C) Photograph of steep foreset laminations (bedding parallel to base of photograph), showing 9 cm scale bar at location of petrographic measurements of mean grain size in D. (D) Mean grain size as a function of stratigraphic height in sample of foreset laminations, showing relatively constant value of 200 µm.

More than 90% of the values recorded from the bottom of unit K to the unit C carbonate are positive, averaging 1.5‰, with a standard deviation of 1.2‰. The scatter in values within individual carbonate intervals is approximately the same as variations in the average values between carbonate intervals (Fig. 7). However, the variation in $\delta^{13}C$ values with stratigraphic position within each relatively thin carbonate interval does not appear to be entirely random (Fig. 10). For example, carbonates from units C and the lower part of unit K show decreasing $\delta^{13}C$ values stratigraphically upward (R^2 = 0.74, 0.88 respectively), whereas values from the lower two carbonates in unit H and the upper carbonate interval in unit J suggest increasing $\delta^{13}C$ values stratigraphically upward (R^2 = 0.26–0.83).

Oxygen isotope ratios range from a low of –16.0‰ (VPDB) to a high of –5.0‰, with an average value of –9.4‰ (Table S1 [footnote 1]). There is no general trend in the mean values for each individual carbonate interval with stratigraphic position (Fig. 7C). The range of values within the carbonate intervals is as great as 6‰, i.e., greater than the variation of mean values for each interval. Correlation of $\delta^{18}O$ and $\delta^{13}C$ is poor for the data set as a whole (Fig. 11). Plots of $\delta^{18}O$ versus stratigraphic position and side-by-side comparison with $\delta^{13}C$ values

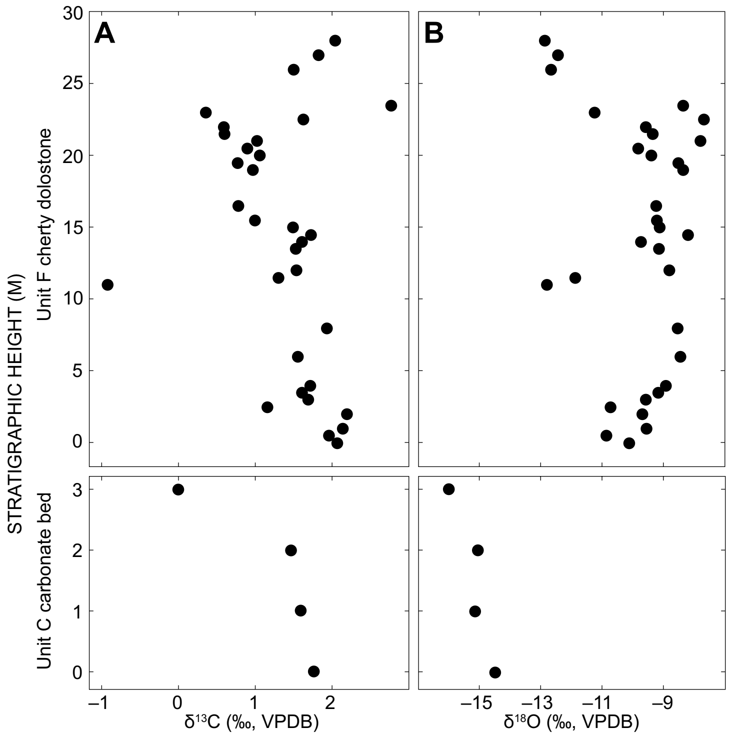

Figure 9. (A) Carbon and (B) oxygen isotope ratios in carbonate as a function of stratigraphic position for units C and F in the Johnnie Wash area. Numerical values are found in Table S1 (text footnote 1). VPDB—Vienna Peedee belemnite.

are presented in the Supplemental Items (Fig. S2 [footnote 1]). Correlation of $\delta^{18}O$ values with stratigraphic position within each interval is also generally poor. Of 12 beds with more than three samples, $R^2 > 0.5$ only for beds Zjj1, Zji2, and Zjc (see Table 1 for nomenclature). With regard to correlation of $\delta^{18}O$ with $\delta^{13}C$, only the carbonate in unit C shows good positive correlation ($R^2 = 0.9$), but this interval only has four data points. Intervals with 10 or more data points all show poor ($R^2 < 0.1$) intrabed correlation of $\delta^{18}O$ with $\delta^{13}C$ (Fig. S2 [footnote 1]).

Subsidence Analysis

Our analyses focused on modeling the tectonic component of subsidence for strata in the Spring Mountains section: Johnnie unit A through the Devonian Devils Gate Formation (Table 1). The model results define the relationship between the stratigraphic thickness *S*, and the tectonic component of subsidence *Y* (Table 2), which yields a resulting curve for the function *Y*(*S*) (Fig. 12). This curve depends on parameters that describe lithification and isostatic adjustment due to sediment loading (Tables 2 and 3), and it is independent of time (Eqs. 1 and 2 *in* Steckler and Watts, 1978). We model the time dependence of subsidence in the Discussion section below.

Our determinations of *Y*(*S*) include the effects of some 3000 m of Mississippian through Triassic overburden that lay above the Johnnie–Devils Gate interval during Jurassic and Early Cretaceous time (Giallorenzo et al., 2017). They also include two major sources of uncertainty. The first is the possible effect of a significant sedimentary substrate, predating Johnnie unit A, on the calculated tectonic subsidence. The substrate may either have been: (1) limited to the Noonday Formation or its equivalents, which are at most a few hundred meters thick and may be represented by the lowest units of the Johnnie Wash section (values Y_{ns} indicate "no substrate"); or (2) a thick succession of Proterozoic Pahrump Group strata (Crystal Spring through Kingston Peak Formations), which could be present at depth beneath the northwest Spring Mountains (values Y_{ws} indicate "with substrate"; note that in Fig. 12, Y_{ws} values were plotted using the base of the Spring Mountains section as a datum for zero, for a direct comparison to Y_{ns}). The oldest Pahrump Group strata, the Crystal Spring Formation, were ~500 m.y. old in Ediacaran time, and therefore these models may somewhat overestimate the effect of sedimentary substrate on late Cryogenian–Ediacaran subsidence. The second major source of uncertainty lies in the resulting density of the delithified sediment column (Bond and Kominz, 1984; Bond et al., 1988). We simulated this error by varying sediment grain density by ±5%, and we note that the effect of sediment unloading is such that the lowest assumed density results in the highest tectonic component of subsidence, and vice versa. This density range yields variations in values of *Y* for a given *S* (Y_{low} or Y_{high}; Table 4) that are similar to those obtained by Bond and Kominz (1984) and Levy and Christie-Blick (1991).

The resulting plots for *Y*(*S*) (Fig. 12) show a decreasing ratio of tectonic subsidence per meter of sediment thickness, with slopes ($\Delta Y/\Delta S$) ranging from values near 1.0 at the base of the section for the "no substrate" curves, to as little as 0.1 near the middle of the section for the "with substrate" curve. More typically, slopes range from 0.3 to 0.6. There is an abrupt change in slope at $S \approx 3500$ m, where the section transitions from predominantly siliciclastic to predominantly carbonate sedimentation. On the no-substrate curve, the slopes defined by the five values closest to $S = 3500$ m are 0.5 ($S < 3500$ m) and 0.2 ($S > 3500$ m), with each of the two arrays appearing quite linear. Corresponding values on the "with substrate" curve are 0.4 and 0.1. Thus, although there is a degree of gradual curvature above and below $S = 3500$ m, most of the flattening of *Y*(*S*) is associated with the lithologic transition.

The effect of including a thick substrate of Pahrump Group strata is to greatly reduce our estimate of *Y* for any given *S*. In other words, by not accounting for the substrate, we overestimate the tectonic component of subsidence by 50% or more, particularly in the early phases of subsidence. Physically, the reason for this is that the no-substrate model inadvertently places incompressible basement rocks where a compacting substrate exists in the event that there is substrate, and therefore the model incorrectly assigns the compaction of the substrate to tectonic subsidence, resulting in an overestimate.

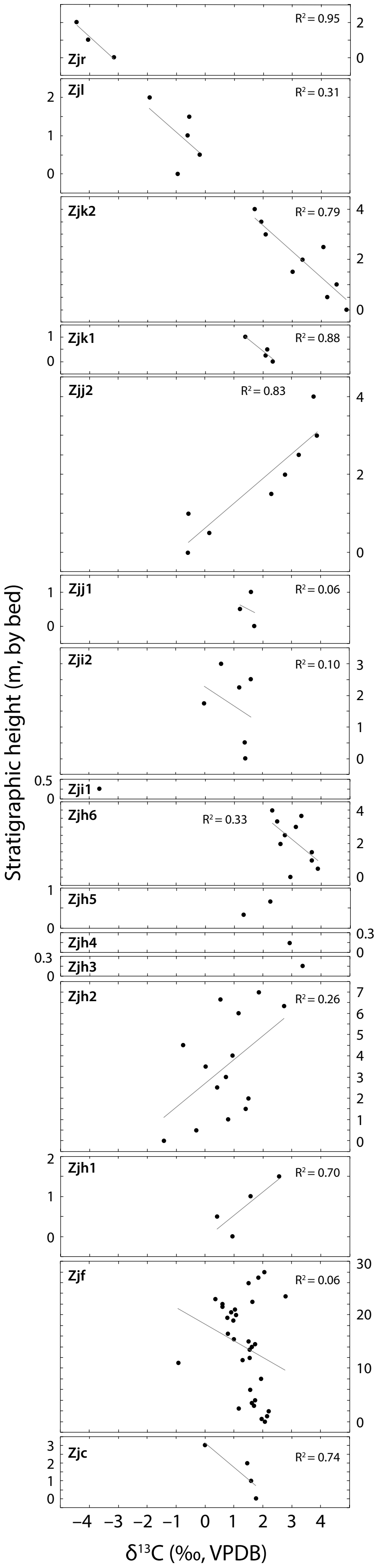

Figure 10. Carbon isotope ratios as function of stratigraphic position, expanding the vertical scale within each carbonate bed to reveal any intrabed trends. Beds are numbered from bottom to top within a given unit, e.g., Zjj1 is the lowest carbonate bed in unit J. VPDB—Vienna Peedee belemnite.

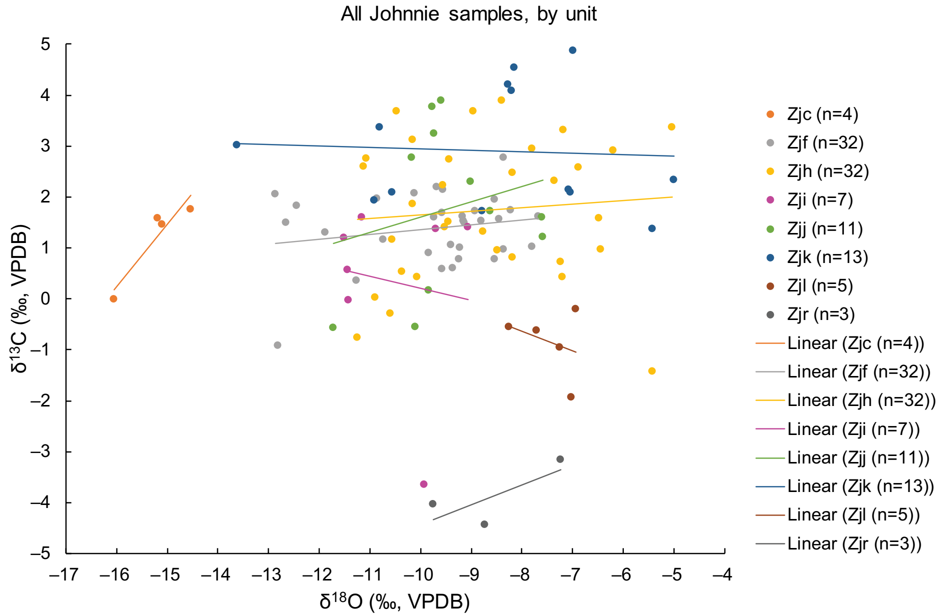

Figure 11. Cross plot of $\delta^{18}O$ vs. $\delta^{13}C$, color coded by stratigraphic unit, showing linear regression lines. VPDB—Vienna Peedee belemnite.

The uncertainties in *Y* due to sediment grain density are generally in the ±10%–15% range. In addition, to the extent that a thick sedimentary substrate is present below the lowest exposures of the Johnnie Formation in Johnnie Wash, tectonic subsidence may be overestimated by several tens of percent. Despite the sensitivity of both the density and substrate effects on the absolute value of *Y*, as we will discuss in the next section, the effect on estimating the age of tectonic subsidence is not large, because these estimates depend mainly on relative, not absolute values of *Y*. Specifically, (1) errors arising from density and substrate are correlated, such that *Y*(*S*) retains its shape even though *Y* may vary significantly; and (2) the exponential equation describing the time dependence of *Y* is defined by ratios between values of *Y*, rather than their absolute magnitudes.

DISCUSSION

Perhaps the most basic question in regard to the origin of the Johnnie Formation is whether the sub-oolite interval contains recognizable subunits that can be correlated across its region of exposures, and the extent to which the section contains major unconformities. These issues are best addressed through lithostratigraphic characteristics and comparisons between the Spring Mountains section and the two other major sections in the region, the Desert Range to the north and the Nopah Range to the south. A second important question is whether or not the sub-oolite (sub–Shuram excursion) interval is a chemostratigraphic correlative with the sub–Shuram excursion Khufai Formation in Oman. A third significant issue is whether continuous Johnnie Formation (and subsequent) deposition occurred through most or all of Ediacaran time, because this aspect is critical to dating the Johnnie Formation using thermal subsidence modeling. A time-dependent exponential thermal subsidence model applied to our decompacted and backstripped subsidence model, *Y*(*S*) (Fig. 12), implies continuous sedimentation along the southwest Laurentian passive margin through the whole of Ediacaran time (i.e., from basal Noonday to early Wood Canyon time, or 635–541 Ma). If such a model is correct, it provides an independent estimate of the age and duration of the Shuram excursion, and whether or not it occurred near the time of the Gaskiers glaciation.

Lithostratigraphy

Although lithostratigraphic correlation of sub–Rainstorm Member Johnnie Formation units is not as straightforward as for the overlying intervals, neither is it particularly complex. The two thickest sections, which both lie in Nevada, the northern part of the Johnnie outcrop belt, include the northern Spring Mountains and Desert Range sections. Both sections are readily divisible into alternating sand-rich and siltstone/carbonate-rich intervals,

TABLE 1. NOMENCLATURE OF STRATIGRAPHIC UNITS USED IN SUBSIDENCE ANALYSIS TABLES

Stratigraphic unit: can be partitioned/combined formations (Fm) and/or members (Mbr)	Abbreviation
Spring Mountains section	
Carbonate overburden	MzPzco
Devils Gate Fm	Ddg
Nevada Fm	Dn
Laketown Fm (upper 50%)	Dl
Laketown Fm (lower 50%)	Sl
Ely Springs Fm	Oes
Eureka Fm	Oe
Pogonip Group (upper third)	Op2
Pogonip Group (lower two thirds)	Op1
Nopah Fm (upper third)	O€n2
Nopah Fm (lower two thirds)	O€n1
Dunderberg Fm	€d
Bonanza King Fm (Banded Mountain Mbr, upper 36%)	€bk2
Bonanza King Fm (Mbrs: Papoose Lake & Banded Mountain, lower 64%)	€bk1
Carrara Fm (upper two thirds)	€c2
Carrara Fm (lower third)	€c1
Zabriskie Fm	€z
Wood Canyon Fm (Ediacaran-Cambrian boundary to top)	€Zwc2
Wood Canyon Fm (to Ediacaran-Cambrian boundary)	€Zwc1
Stirling Fm (members A through E)	Zsa - Zse
Johnnie Fm (Rainstorm Mbr, oolite bed's base to top of Mbr)	Zjr2
Johnnie Fm (Rainstorm Mbr, base to oolite bed's base)	Zjr1
Johnnie Fm (members A through L)	Zja - Zjl
Pahrump Group substrate (hypothetical)	
Johnnie Fm (presumed equivalent to the Transitional Mbr of Stewart, 1970)	Zjt
Kingston Peak Fm (Mbr: South Park, sub-Mbr: Wildrose)	Zkpw
Kingston Peak Fm (Mbr: South Park, sub-Mbr: Thorndike)	Zkpth
Kingston Peak Fm (Mbr: South Park, sub-Mbr: Mountain Girl)	Zkpmg
Kingston Peak Fm (Mbr: South Park, sub-Mbrs: Sourdough & Middle Park)	Zkpsmp
Kingston Peak Fm (Limekiln-Surprise Mbr)	Zkpls
Beck Springs Fm/Kingston Peak Fm (lower)	Zbs
Horse Thief Springs Fm	Zhs
Crystal Springs Fm (upper)	Ycs2
Crystal Springs Fm (lower)	Ycs1

TABLE 2. NOMENCLATURE FOR PARAMETERS USED IN DELITHIFICATION AND BACKSTRIPPING ANALYSIS†

ϕ_0	Surface porosity (%)
c	Porosity depth coefficient (km^{-1})
ρ_{sg}	Sediment grain density (kg m^{-3})
h	Stratigraphic thickness (m)
S	Cumulative stratigraphic thickness (m)
S^*	Delithified/decompacted thickness (m)
Y	Tectonic subsidence (m)

†Subscripts for *S*, *S**, and *Y*: ns—no Pahrump Group substrate; ws—with Pahrump Group substrate; low—low subsidence, using +5% ρ_{sg}; high—high subsidence, using –5% ρ_{sg}.

each on the order of 100 m to a few hundred meters thick (I, II, III in Fig. 13 on the northern Spring Mountains section). The three sand-rich intervals of the Johnnie Formation are succeeded by four additional sand-rich intervals that have long been recognized as regionally correlative units (IV–VII in Fig. 13 on the northern Spring Mountains section), of which the top three have paleontological age constraints. The two sections each contain three sand-rich intervals below the Rainstorm Member that have proportionate relative thicknesses. Further, the siltstone/carbonate-rich interval between sand-rich intervals II and III contains an ~40-m-thick cherty dolostone unit in both sections, strengthening correlation, as noted by Stewart (1970) and Benmore (1978). We correlate sand-rich interval I of the Spring Mountains (unit B) with

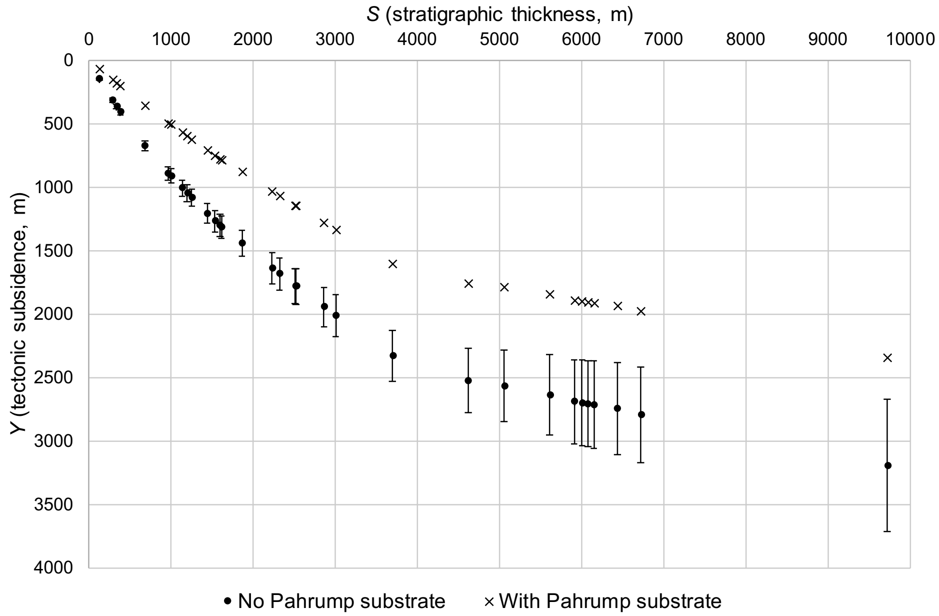

Figure 12. Plot showing calculated tectonic subsidence (*Y*) as a function of observed stratigraphic thickness (*S*). Lower curve shows results assuming unit A of the Johnnie Formation at the type locality is immediately underlain by crystalline basement. Error bars show range of estimates for *Y* produced by a ±5% variation in sediment grain density. Upper curve shows results assuming unit A is underlain by ~2000 m of hypothetical Pahrump Group strata.

the Carbonate member in the Desert Range section, on the basis of stratigraphic position. We note, however, that the pervasive soft sediment deformation in unit B has not been reported from orthoquartzites in the Carbonate member, and that unit B does not contain carbonate. Unit A, which is predominantly siltstone, would therefore correlate with siltstones and oolitic limestones underneath the Carbonate member. The oolitic limestone unit at the base of the Desert Range section has been considered to be correlative with the Noonday Formation (Longwell et al., 1965; Gillett and Van Alstine, 1982), implying that unit A in the Spring Mountains may also be a Noonday correlative (Fig. 13).

The southern Nopah Range section is approximately half the thickness of the northern Spring Mountains and Desert Range sections, and it contains a number of subaerial erosion surfaces that thus far have not been observed in the thicker Nevada sections (Summa, 1993). Like the Nevada sections, however, it does contain three sub–Rainstorm Member sand-rich intervals, suggesting lithostratigraphic correlation (Fig. 13). Specifically, the lower part of the Transitional, Quartzite, and Upper carbonate-bearing members of Stewart (1970) would correspond to sand-rich intervals I, II, and III, respectively, in the Spring Mountains. The correlation is strengthened by: (1) the alternating orthoquartzite/carbonate cycles evident in sand-rich interval III in both the northern Spring Mountains and southern Nopah Range sections; (2) the lack of carbonate and abundance of high-angle cross-stratification in interval II in all three sections (Quartzite member = upper part of Lower quartzite and siltstone member = unit D, Fig. 13); (3) the consistency of unimodal, south-southwest–directed paleoflow directions in pre–Rainstorm Member orthoquartzites in the Spring Mountains and Desert Range sections (Fig. 14); and (4) the lithological similarity between the lowest sand-rich intervals in the southern Nopah Range and Desert Range sections, both of which contain a mixed carbonate-siliciclastic assemblage. Militating against these lithostratigraphic correlations are the observations that: (1) the interval III correlative in the Desert Range lacks carbonate; (2) interval I in the Spring Mountains (unit B) also lacks carbonate; and (3) the proposed Noonday substrate of interval I is lithostratigraphically dissimilar in all three sections, ranging from pale-gray quartz-rich dolomite boundstone in the Nopah Range, to phyllitic siltstone in the Spring Mountains, to medium-gray oolitic limestone in the Desert Range. Regardless of the details of these correlations, the most important facets of the two sections in Nevada are the following: (1) The sub–Rainstorm Member sections are at least twice as thick as the Nopah Range section; and (2) evidence for subaerial erosion, such as grikes, paleosols, channel scour, and desiccation cracks, which is conspicuous in the Nopah Range section, appears to be lacking. Although significant depositional hiatuses within the Nevada sections cannot be ruled out, the overall lithostratigraphic uniformity or "monotony" of these sections (siltstone and fine- to medium-grained sandstone and orthoquartzite, with sporadic thin carbonate beds) is consistent with conformable sedimentation on a stably subsiding continental shelf (Stewart, 1970; Fedo and Cooper, 2001; Schoenborn et al., 2012).

TABLE 3. PARAMETERS USED IN DELITHIFICATION AND BACKSTRIPPING ANALYSIS OF THE SPRING MOUNTAINS SECTION[†]

Unit	Age[§] (Ma)	Lithology	ϕ_0 (%)	c (km^{-1})	ρ_{sg} (kg m^{-3})	h (m)	S_{ns} (m)	S_{ws} (m)
MzPzco[#]	Ca. 243	l/d	43	0.58	2785	3000	9720	11745
Ddg	359	d	43	0.58	2710	286	6720	8745
Dn	383	d	43	0.58	2860	286	6434	8459
Dl	393	d	43	0.58	2860	71.5	6148	8173
Sl	419	d	43	0.58	2860	71.5	6076.5	8101.5
Oes	444	d	43	0.58	2860	95	6005	8030
Oe	458	s	49	0.27	2650	71	5910	7935
Op2	–	l	43	0.58	2710	230	5839	7864
Op1**	470	l	43	0.58	2710	460	5609	7634
OЄn2	–	d	43	0.58	2860	95	5149	7174
OЄn1	485	d	43	0.58	2860	191	5054	7079
Єd	–	sh	63	0.51	2720	48	4863	6888
Єbk2	–	d	43	0.58	2860	197	4815	6840
Єbk1	497	d	43	0.58	2860	637	4618	6643
Єc2	–	sh	63	0.51	2720	286	3981	6006
Єc1	509	sh	63	0.51	2720	143	3695	5720
Єz	–	s	49	0.27	2650	24	3552	5577
ЄZwc2	–	s/slt	49	0.27	2650	523	3528	5553
ЄZwc1	541	s/slt	49	0.27	2650	144	3005	5030
Zse	–	s	49	0.27	2650	340	2861	4886
Zsd[††]	–	d	46	0.43	2755	10	2521	4546
Zsc	–	slt/s	49	0.27	2650	190	2511	4536
Zsb	–	s/slt	49	0.27	2650	90	2321	4346
Zsa	–	s	49	0.27	2650	369	2231	4256
Zjr2[§§]	–	slt/s/l/d	47	0.37	2695	250	1862	3887
Zjr1[##]	–	slt	49	0.27	2650	17	1612	3637
Zjl	–	s/slt	49	0.27	2650	60	1595	3620
Zjk	–	s/slt	49	0.27	2650	95	1535	3560
Zjj	–	s/slt	49	0.27	2650	190	1440	3465
Zji	–	s/slt	49	0.27	2650	55	1250	3275
Zjh	–	s/slt	49	0.27	2650	60	1195	3220
Zjg	–	slt	49	0.27	2650	135	1135	3160
Zjf***	–	d	43	0.58	2860	40	1000	3025
Zje	–	s/slt	49	0.27	2650	280	960	2985
Zjd[†††]	–	s	49	0.27	2650	300	680	2705
Zjc2	–	slt	49	0.27	2650	45	380	2405
Zjc1[§§§]	–	slt	49	0.27	2650	50	335	2360
Zjb[###]	–	s	49	0.27	2650	160	285	2310
Zja	–	slt	49	0.27	2650	125	125	2150
Zjt****	–	d/s	46	0.43	2755	125	–	2025
Zkpw[††††]	635	ss	49	0.27	2650	100	–	1900
Zkpth	–	d	43	0.58	2860	100	–	1800
Zkpmg	–	s	49	0.27	2650	100	–	1700
Zkpsmp	–	slt	49	0.27	2650	200	–	1600
Zkpls	–	s/cgl	49	0.27	2650	400	–	1400
Zbs	–	d	43	0.58	2860	200	–	1000
Zhs[§§§§]	<787	s	49	0.27	2650	200	–	800
Ycs2	>1087	d	43	0.58	2860	200	–	600
Ycs1[####]	–	s	49	0.27	2650	400	–	400

[†]Values from table 9.1 *in* Allen and Allen (2005), Equation 3 *in* Halley and Schmoker (1983), Deer et al. (1992), or weighted averages for lithologic mixtures. Abbreviations for lithology are: s—sandstone; slt—siltstone; l—limestone; d—dolostone; sh—shale; cgl—conglomerate. See Table 2 for parameter definitions.

[§]Ages are at top of unit.

[#]Lithologic ratio used is 50/50; average for ρ_{sg}.

**Carbonate is mostly limestone (fig. 2 *in* Burchfiel et al., 1974) .

[††]Dolostone is sandy (stratigraphic column for Spring Mountains, plate 2 *in* Stewart, 1970).

[§§]Shuram excursion ends. Lithologic ratio is slt+s/l/d = 67/16.5/16.5 (table 3 *in* Stewart, 1970).

[##]Shuram excursion begins.

***Cherty dolostone.

[†††]High-angle cross-bedding.

[§§§]Onset of thermal subsidence (based on interpretation of ball-and-pillow structure; see text).

[###]Ball-and-pillow structure.

****Lithologic ratio is d/s = 50/50.

[††††]Age from Petterson et al. (2011).

[§§§§]Maximum age from Mahon et al. (2014).

[####]Minimum age from Heaman and Grotzinger (1992).

Research Paper

TABLE 4. RESULTS FROM DELITHIFICATION AND BACKSTRIPPING ANALYSIS OF THE SPRING MOUNTAINS SECTION†

Unit	Age§ (Ma)	S_{ns}	S^*_{ns}	$Y_{ns, low}$	Y_{ns}	$Y_{ns, high}$	S_{ws}	S^*_{ws}	$Y_{ws, low}$	Y_{ws}	$Y_{ws, high}$
MzPzco	Ca. 243	9720	9714	2670	3193	3715	11745	11736	3128	3768	4406
Ddg	359	6720	7489	2412	2791	3169	8745	9548	2905	3401	3895
Dn	383	6434	7246	2380	2743	3105	8459	9310	2878	3358	3836
Dl	393	6148	7002	2367	2713	3058	8173	9071	2871	3334	3795
Sl	419	6076.5	6940	2364	2706	3046	8101.5	9011	2869	3328	3785
Oes	444	6005	6881	2361	2699	3035	8030	8953	2868	3322	3776
Oe	458	5910	6799	2357	2689	3020	7935	8874	2866	3315	3763
Op2	–	5839	–	–	–	–	7864	–	–	–	–
Op1	470	5609	6541	2320	2636	2950	7634	8622	2836	3269	3700
OЄn2	–	5149	–	–	–	–	7174	–	–	–	–
OЄn1	485	5054	6070	2280	2564	2846	7079	8167	2811	3212	3611
Єd	–	4863	–	–	–	–	6888	–	–	–	–
Єbk2	–	4815	–	–	–	–	6840	–	–	–	–
Єbk1	497	4618	5694	2264	2522	2778	6643	7804	2809	3183	3556
Єc2	–	3981	–	–	–	–	6006	–	–	–	–
Єc1	509	3695	4798	2125	2327	2528	5720	6949	2710	3029	3347
Єz	–	3552	–	–	–	–	5577	–	–	–	–
ЄZwc2	–	3528	–	–	–	–	5553	–	–	–	–
ЄZwc1	541	3005	4024	1844	2009	2173	5030	6220	2475	2757	3037
Zse	–	2861	3865	1786	1943	2100	4886	6072	2428	2702	2975
Zsd	–	2521	3481	1642	1781	1919	4546	5718	2313	2570	2824
Zsc	–	2511	3469	1638	1777	1914	4536	5708	2311	2566	2821
Zsb	–	2321	3250	1553	1682	1809	4346	5507	2245	2490	2735
Zsa	–	2231	3144	1512	1635	1758	4256	5411	2213	2454	2693
Zjr2	–	1862	2706	1337	1441	1544	3887	5018	2083	2304	2523
Zjr1	–	1612	2400	1221	1311	1399	3637	4748	2004	2210	2415
Zjl	–	1595	2379	1212	1301	1388	3620	4730	1997	2203	2407
Zjk	–	1535	2303	1179	1264	1349	3560	4663	1973	2176	2377
Zjj	–	1440	2179	1125	1204	1284	3465	4556	1936	2133	2329
Zji	–	1250	1930	1012	1082	1150	3275	4343	1859	2046	2231
Zjh	–	1195	1856	978	1045	1110	3220	4280	1836	2020	2203
Zjg	–	1135	1775	941	1004	1066	3160	4212	1812	1992	2171
Zjf	–	1000	1589	853	909	964	3025	4058	1756	1929	2101
Zje	–	960	1537	835	889	941	2985	4015	1747	1918	2087
Zjd	–	680	1132	633	671	709	2705	3689	1624	1779	1933
Zjc2	–	380	664	385	406	427	2405	3331	1486	1624	1762
Zjc1	–	335	591	344	363	382	2360	3278	1465	1601	1736
Zjb	–	285	507	297	313	329	2310	3217	1441	1574	1707
Zja	–	125	230	138	145	152	2150	3024	1365	1489	1612
Zjt	–	–	–	–	–	–	2025	2871	1304	1422	1538
Zkpw	635	–	–	–	–	–	1900	2722	1255	1365	1475
Zkpth	–	–	–	–	–	–	1800	2597	1204	1308	1412
Zkpmg	–	–	–	–	–	–	1700	2480	1173	1271	1368
Zkpsmp	–	–	–	–	–	–	1600	2349	1116	1209	1300
Zkpls	–	–	–	–	–	–	1400	2086	1000	1081	1162
Zbs	–	–	–	–	–	–	1000	1546	756	815	873
Zhs	<787	–	–	–	–	–	800	1288	669	716	762
Ycs2	>1087	–	–	–	–	–	600	993	523	558	593
Ycs1	–	–	–	–	–	–	400	707	408	431	453

†See Table 2 for parameter definitions.
§Ages are at top of unit.

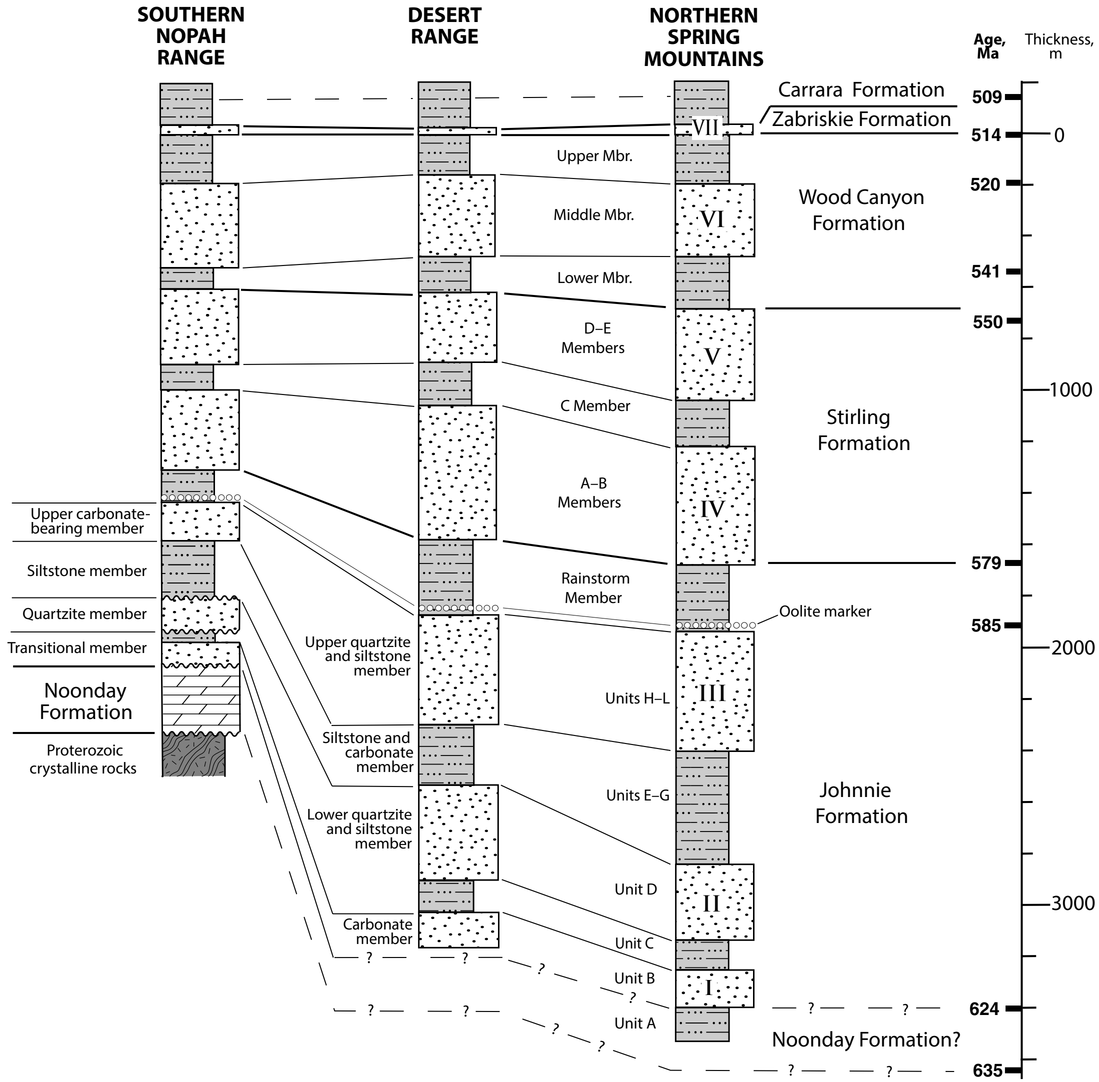

Figure 13. Lithostratigraphic columns of the Johnnie Formation and enveloping Ediacaran–Cambrian formations at three key localities in Nevada and California, indicating the stratigraphic distribution of sand-rich intervals versus siltstone/carbonate-rich intervals. Informal member and unit designations in the southern Nopah and Desert Range sections are after Stewart (1970); note that the informal "Carbonate member" in the Desert Range section is predominantly sand-rich carbonate and fine- to medium-grained orthoquartzite with no siltstone. Bold numbers to the left of the scale bar are ages in Ma as follows: 509—base of Middle Cambrian (Palmer and Halley, 1979); 514 and 520—base of *Bonnia-Olenellus* and *Fallotaspis* trilobite zones, respectively (Hunt, 1990; Hollingsworth, 2005); 541 and 550—base of Cambrian and first-appearance datum of cloudinids (Corsetti and Hagadorn, 2000; Smith et al., 2016; Narbonne et al., 2012); 579, 585, and 624—model age estimates from this study; 635—base of Ediacaran (Petterson et al., 2011). Roman numerals indicate sand-rich intervals beginning with unit B of the type Johnnie Formation.

The pervasive ball-and-pillow and other paleoliquefaction structures in sand-rich interval I (unit B) are most simply interpreted as reflecting a period of high sediment flux during early Johnnie Formation deposition. These structures may have significance for the timing of the transition from mechanical stretching of the lithosphere to purely thermal subsidence, because (1) rapid subsidence is characteristic of both the rift phase and early thermal subsidence phase of passive-margin formation (e.g., Sawyer et al., 1982), and (2) such structures could be evidence for seismic shaking (e.g., Sims, 2012). The observation that essentially the entire 160 m thickness of unit B is affected implies that, whatever its cause, it was persistent over a sustained period of time. The other significant observation is that with only one exception, paleoliquefaction structures do not appear anywhere else higher in the section, despite

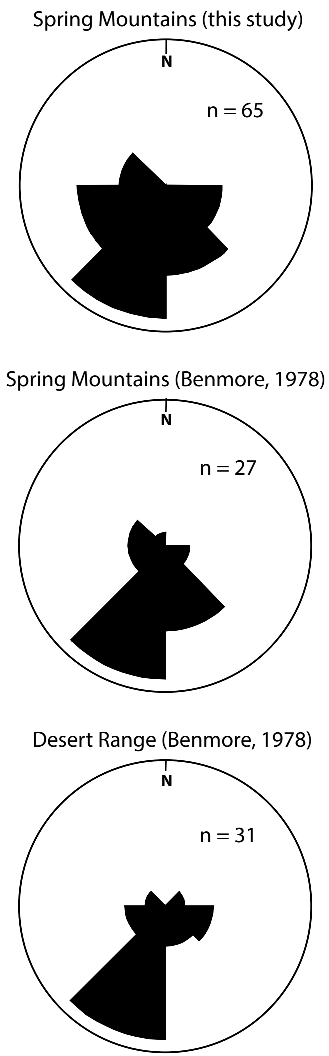

Figure 14. Paleoflow rosettes showing foreset lamination dip directions, corrected for bedding dip. Upper two rosettes compare data from sand-rich interval II (Fig. 8B) with data from all subunit H strata (p. 224 in Benmore, 1978). Bottom rosette shows data from all pre–Rainstorm Member orthoquartzites in the Desert Range (p. 221 in Benmore, 1978).

the ubiquity of meter-scale interbeds of fine- to medium-grained sandstone overlying fine-grained sandstone or siltstone throughout the section. Thus, the cause (or causes) of soft-sediment deformation appears to be temporally restricted to, at most, sand-rich interval I and enveloping siltstone units A and C, and it presumably ended by the time of deposition of sand-rich interval II (unit D). If it is assumed that the cause is earthquakes, then sand-rich intervals I and II record a transition from frequent seismic shaking to apparent seismic quiescence. Such an interpretation is consistent with previous suggestions that the end of mechanical stretching may have occurred near the base of the Johnnie Formation (Summa, 1993; Fedo and Cooper, 2001; Schoenborn et al., 2012). A ready alternative to a seismic trigger, however, is the effect of pressure contrasts from storm waves, which have also been shown to induce liquefaction and soft sediment deformation, including ball-and-pillow structure (Alfaro et al., 2002).

Chemostratigraphy

A composite plot of $\delta^{13}C$ values of carbonate from the Johnnie Formation in southwest Laurentia (Verdel et al., 2011; this study) yields an overall pattern that is similar to profiles in Oman that contain the Shuram excursion, including a period of positive values as high as 4‰–6‰, rapid descent to values as low as –11‰ to –12‰, and a more gradual rise back to positive values (Fig. 15). The uniformly positive $\delta^{13}C$ values below the excursion in southwest Laurentia, generally of 1‰–3‰, invite detailed comparison with chemostratigraphic profiles in the carbonate-rich Khufai Formation in Oman, which lies immediately below the type Shuram excursion. The stratigraphic thickness of units between the zero crossings of the Shuram excursion in Oman and southwest Laurentia are similar, ~500–700 m (Verdel et al., 2011). We therefore compared our profile to those from Oman without any modification to the vertical scaling (stratigraphic height), fixing the zero crossings at the base of the Shuram excursion at the same height. The Khufai sections in general are positive in $\delta^{13}C$ and show considerable variation, depending on the degree of diagenetic alteration. In least-altered sections (Mukhaibah Dome area), maximum values range up to 6‰, averaging 4‰–5‰ (Fig. 16A), i.e., considerably more positive than the Johnnie Formation profile. In more-altered sections (Buah Dome area; Fig. 16B), the profiles are quite similar to that of the Johnnie Formation. Given the close correspondence between the Johnnie profile and most of the Oman profiles (Fig. S3 [footnote 1]), we conclude that the data are consistent with, but do not absolutely demonstrate, temporal correlation between the upper part of the sub–Rainstorm Member Johnnie Formation (units H through L in the Spring Mountains) and the Khufai Formation.

The least-altered Khufai sections are generally considered to be representative of seawater carbon isotopic composition, defining a prolonged interval of $\delta^{13}C$ values in seawater near 6‰. Therefore, it seems clear that subsequent diagenesis was primarily responsible for reducing $\delta^{13}C$ values, in both Oman and the sub–Rainstorm Member Mount Schader section, by as much as 4‰–5‰. In the Pleistocene environment, such reduction has been shown to result from carbon isotopic exchange between carbonate beds and meteoric water, often resulting in $\delta^{13}C$ values decreasing stratigraphically upward at the scale of a few meters in beds exposed to erosion (Allan and Matthews, 1977, 1982; Quinn, 1991; Melim et al., 1995, 2001). The strong intrabed variations in $\delta^{13}C$ values in 1–2-m-thick carbonate intervals in the Johnnie Formation (Fig. 10) could potentially be explained by this mechanism, although $\delta^{13}C$ values of meteoric water at that time are poorly constrained and may not have been as

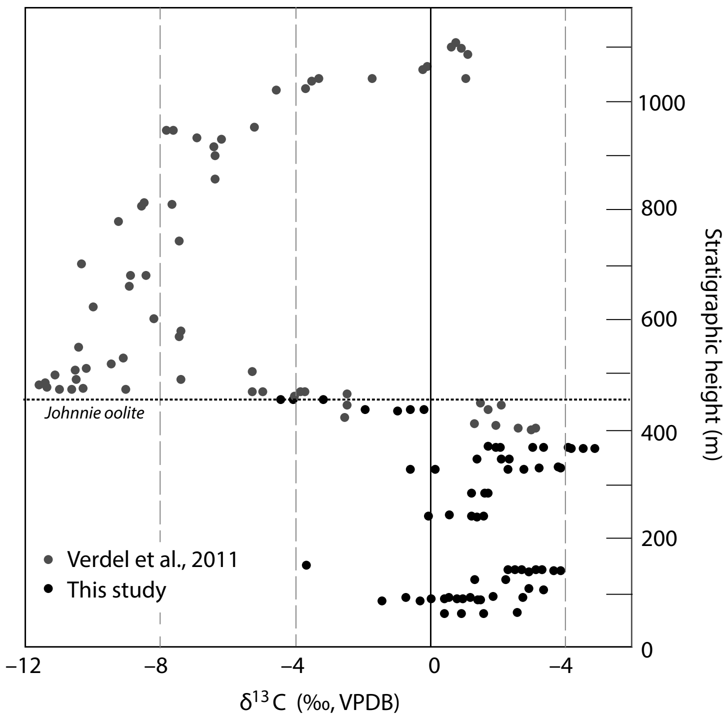

Figure 15. Composite chemostratigraphy of the upper Johnnie Formation, showing carbon isotopic ratios in carbonate from unit H up to the oolite marker horizon in the lowermost Rainstorm Member (Mount Schader section, this study) and values from just below the base of the Rainstorm Member to the top of the member (southern Panamint Range; Verdel et al., 2011). VPDB—Vienna Peedee belemnite.

strongly negative as modern values. Further, the intrabed trends in $\delta^{13}C$ values both increase and decrease downward, and there is no evidence of subaerial exposure on the tops of any of the beds. As with most Neoproterozoic carbonates, determining the mechanisms of depletion of $\delta^{13}C$ values and their relationship to diagenetic textures and the biosphere is a difficult and controversial issue (Knauth and Kennedy, 2009; Derry, 2010a, 2010b; Grotzinger et al., 2011), and it is beyond the scope of this paper to resolve. One thing we can say, however, about the Mount Schader data set is that it displays no clear correlations between $\delta^{18}O$ and $\delta^{13}C$ (Fig. 11), as predicted by various isotopic exchange models (fig. 4 *in* Osburn et al., 2015). Despite this controversy, the good match between the type Johnnie Formation sub–Rainstorm Member section and the Khufai Formation supports the hypothesis that regardless of the origin of the anomalies, they nonetheless appear to be a useful correlation tool (Grotzinger et al., 2011). Tectonic reconstructions of the Neoproterozoic continent Rodinia put both the Shuram and the Johnnie formations roughly at the equator in Ediacaran time, but the two formations were located anywhere from 10,000 to 15,000 km away from each other (Li et al., 2008, 2013), making the isotopic correlation of the Shuram and sub-Shuram intervals all the more impressive.

One of the hallmarks of Neoproterozoic glacial cap carbonates is their frequent occurrence as thin, isolated intervals amid large thicknesses of enveloping strata that are entirely siliciclastic. Below unit H, there are two such isolated carbonate intervals, one in unit C and the other composing the entirety of unit F. Given their stratigraphic position between the Marinoan cap carbonate sequence and the base of the Cambrian, it is possible that either one of these units represents postglacial carbonate "rainout," for example, as might be expected in the more southerly latitudes in the wake of the Gaskiers glaciation at 579 Ma (e.g., Pu et al., 2016). The generally positive $\delta^{13}C$ values in the unit C and unit F carbonates, averaging between 1‰ and 2‰, argue strongly against either of these intervals representing a Gaskiers cap carbonate, which in Newfoundland yielded $\delta^{13}C$ values of –8‰ to –2‰ (Myrow and Kaufman, 1999). Further, textural features widely described from cap carbonates (e.g., sheet cracks, tubes, teepee structures, etc.) are not observed in either of these intervals.

Subsidence Analysis

The substantial thickness of the Johnnie Formation, lack of evidence for unconformities in the Nevada sections, and the strengthened isotopic tie to the type Shuram excursion, motivate the hypothesis that the Noonday through lower Wood Canyon interval records continuous deposition through most or all of Ediacaran time. In the last section, backstripping and decompaction defined tectonic subsidence Y as a function of stratigraphic position S, independent of time. In this section, we model the element of time as exponential subsidence, assuming that Johnnie Formation and subsequent deposition of the passive-margin wedge occurred as a result of conductive cooling of rifted lithosphere. Subsidence analysis with well-defined ages at the Cambrian-Precambrian boundary (541 Ma) and at the base of Cambrian Age 5 (509 Ma) creates a considerably improved basis over previous studies for estimating stratigraphic age in Ediacaran strata by extrapolating the subsidence history back in time.

Regardless of the absolute elevation following mechanical extension of the lithosphere, once thermal subsidence begins, the elevation e of the surface, above its equilibrium value at $t = \infty$, is closely approximated by:

$$e(t) \cong E_0 r e^{-\frac{t}{\tau}}, \qquad (1)$$

where E_0r is the elevation of stretched lithosphere above its equilibrium depth at infinite time (or in the case of infinite stretching, the height of the ocean floor above the abyssal plains), t is time, τ is the characteristic time $\left(\text{time at which } \frac{e}{E_0 r} = \frac{1}{\mathrm{e}}\right)$ and

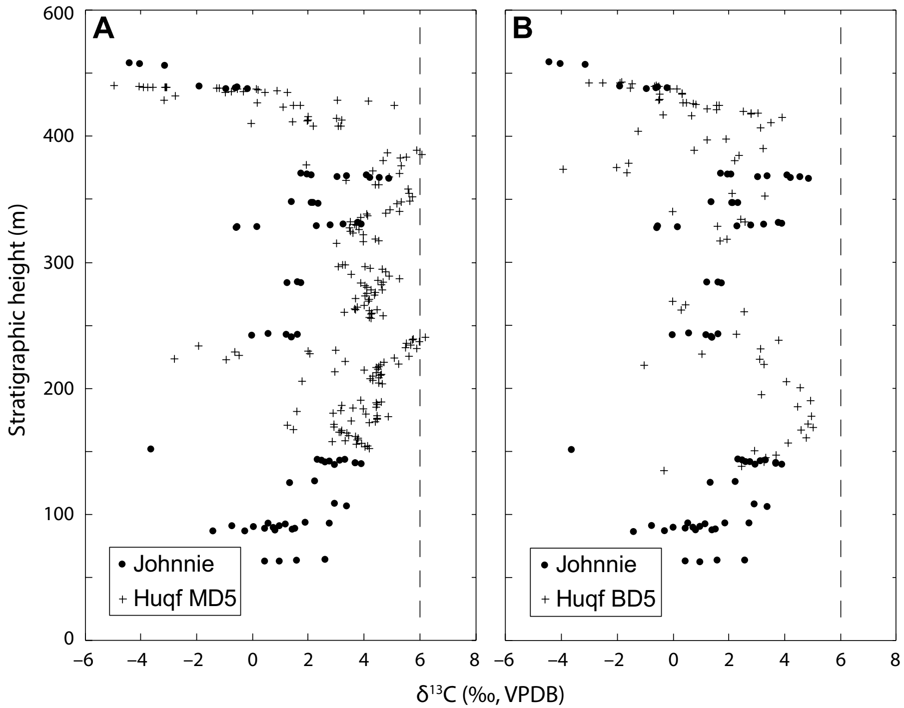

Figure 16. Chemostratigraphic profiles comparing carbon isotopic data from the Johnnie Formation from unit H through the lowermost Rainstorm Member (ending at the top of the oolite marker bed; Fig. 7) with profiles from (A) the Mukhaibah Dome (MD5) and (B) the Buah Dome (BD5) areas of Oman (Osburn et al., 2015). Vertical axis shows measured stratigraphic height in all profiles. Six additional profile comparisons are presented in Figure S3 (text footnote 1). VPDB—Vienna Peedee belemnite.

$$r = \frac{\beta}{\pi}\sin\frac{\pi}{\beta}, \qquad (2)$$

where β is the stretching factor (Fig. 17; see Eqs. 10 and 11 *in* McKenzie, 1978). E_0 and r are not parameters of interest when using subsidence as a chronometer, because we are attempting to use the late history of postrift subsidence, which is well dated, to constrain the earlier history of postrift subsidence, which is not. The simple exponential formula for elevation versus time $e(t)$ of Equation 1 is converted to subsidence depth Y versus time by substituting $(E_0 r - Y)$ for e, yielding:

$$Y(t) \cong E_0 r\left(1 - e^{-\frac{t}{\tau}}\right). \qquad (3)$$

In the case of mid-ocean ridges, where β = ∞ and $r = 1$, $E_0 r$ is empirically shown to be within a few percent of 3.2 km (Parsons and Sclater, 1977). We note that this value does not correspond to the actual ridge elevation above the abyssal plain, which is much higher for oceanic crust less than 20 m.y. old. The characteristic time τ, which depends on the thermal diffusivity and thickness of equilibrium lithosphere, shows somewhat greater variation depending on the ridge (±10% for the best-constrained ridges; table 1 *in* Parsons and

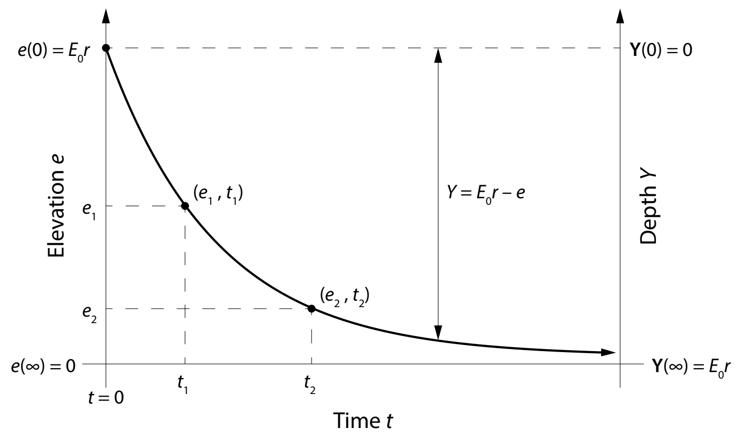

Figure 17. Plot showing an exponential subsidence model $Y(t)$, based on conductive cooling of extended lithosphere (McKenzie, 1978). Plotted on curve are the onset of thermal subsidence at $t = 0$, and two arbitrary points in the history of subsidence. Note that so long as the stratigraphic position of $e(\infty) = 0$ is well defined, the form of the subsidence curve, including the exponential decay constant τ, is uniquely determined and does not depend on $e(0) = E_0 r$.

Sclater, 1977), but a generally accepted range of values in subsidence analyses of passive margins is 50–65 m.y. (McKenzie, 1978; Allen and Allen, 2005). This corresponds to a "half-life" of thermal subsidence of 35–45 m.y. Even though this key parameter may vary significantly, we can estimate τ directly from our subsidence model, as an independent test of the hypothesis that the margin is in a state of exponential thermal subsidence, comparable to well-studied Mesozoic and Cenozoic examples. If our estimate of τ lies significantly outside the range of 50–65 m.y., it would falsify the thermal subsidence hypothesis.

Even though we do not know E_0r, estimation of τ and extrapolation of the curve back in time requires as few as two known elevation-time pairs, (e_1, t_1) and (e_2, t_2) (Fig. 17). Substituting these pairs into Equation 1, differencing the equations, and solving for τ yields:

$$\tau = \frac{(t_2 - t_1)}{\ln\left(\frac{e_1}{e_2}\right)}. \tag{4}$$

The differencing of the two equations eliminates E_0r, and hence the most important parameters in estimating both τ and the thermal subsidence curve itself are the elevation of two points relatively well separated in time from each other, and an estimate of zero elevation, i.e., where $e(\infty) = 0$ or the slope of $Y(t)$ is negligible. The thermal subsidence curve is then presumably applicable back in time to whatever point in the section at which we are still confident that the margin is in a state of pure thermal subsidence. As noted above, this level is probably no higher in the section than the lower part of the Johnnie Formation, and it may be much deeper, perhaps within the upper part of the underlying Pahrump Group.

Temporal constraints on the younger part of the subsidence curve are fairly similar to those used by Levy and Christie-Blick (1991), with the exception of their two oldest points, the base of the Cambrian Age 5 (approximately Middle Cambrian, 509 Ma; Walker et al., 2013) and the base of the Paibian (approximately Upper Cambrian, 497 Ma; Walker et al., 2013), which at the time were estimated to be 540 Ma and 523 Ma, respectively. Critically for this study, both the position and age of the Ediacaran-Cambrian boundary are well defined, lying within the Lower Member of the Wood Canyon Formation with an age of 541 Ma (Corsetti and Hagadorn, 2000). The 541 and 509 Ma constraints thus function as points (e_1, t_1) and (e_2, t_2), respectively, in our initial analysis, defining an exponential subsidence curve. As the oldest reliable temporally constrained points on the curve, they are the strongest constraints on extrapolating the curve back in time.

Points younger than 509 Ma are also well dated. These points clearly postdate the Sauk marine transgression, which marks a transition from predominantly siliciclastic to carbonate sedimentation, due to flooding of the craton through middle and late Cambrian time. Associated with the transgression, the average deposition rate $S(t)$ increases markedly from ~20 m/m.y. from 541 to 509 Ma to ~80 m/m.y. from 509 to 497 Ma (Table 4). Clearly, a fourfold increase in accumulation rate appears incompatible with any form of exponential subsidence. As explained below, the remarkable increase in subsidence rate owes its origin to the combination of sea-level rise and carbonate sedimentation, not renewed tectonism. The important point here is to note that the 541 and 509 Ma data points occur within the Lower Wood Canyon and Lower Carrara formations, respectively, both of which are shallow-water, mixed carbonate-siliciclastic facies associations that were probably deposited at similar points in global sea level. Both were deposited during highstand intervals relative to their transgressive substrates (the Stirling E Member and Zabriskie Formation, respectively). In the case of the Lower Member of the Wood Canyon Formation, the system evolved into a glacial drawdown of sea level (Smith et al., 2016). In the case of the lower Carrara Formation, sea level kept rising to a level that generally exceeded that of Ediacaran–early Cambrian time (Palmer, 1981).

The late subsidence history is characterized by very slow accumulation in Silurian and Early Devonian time (<3 m/m.y.; Table 4), and hence the difference between Silurian and Devonian values of Y compared to those at 541 and 509 Ma provides firm estimates of e_1 and e_2. We note that with these constraints, the precise values of time and elevation for Paibian through Upper Ordovician strata provide little additional constraint on the form of the exponential subsidence curve.

Temporal Model

We present a temporal model of both observed subsidence $S(t)$ (i.e., stratigraphic thickness) and tectonic subsidence $Y(t)$ using a novel mode of presentation that orthogonally projects $Y(t)$ and $t(S)$ onto a graph of the numerically determined function $Y(S)$ (Fig. 18). In this approach, $Y(S)$ is plotted in the upper-left corner, $Y(t)$ is plotted in the upper-right corner, $t(S)$ is plotted in the lower-left corner, and $S(t)$ is plotted in the lower-right corner. The plot shows a simultaneous projection of Y and S onto their respective temporal models, graphically showing the influence of the slope of $Y(S)$ on the observed subsidence rates. The graph shows that, between 509 and 485 Ma, the increase in compressibility of the carbonate sediment [lower slope on $Y(S)$] combined with the accelerated schedule of subsidence caused by the flooding of the craton [higher slope on $Y(t)$] resulted in a dramatic increase in sediment accumulation rate [lower slope on $t(S)$ and higher slope on $S(t)$], even though exponential thermal subsidence was slowly decreasing. This result is critical, because it obviates the primary reason that most previous workers have cited in favor of Cambrian rifting along western Laurentia (e.g., Bond and Kominz, 1984; Levy and Christie-Blick, 1991; Yonkee et al., 2014).

Parameter Estimates and Sensitivities

Estimates of the exponential time constant τ vary according to two main uncertainties, (1) the sediment grain density assumed in our delithification model, and (2) whether or not a thick substrate of Pahrump Group strata is present at depth beneath the exposed Spring Mountains section. We calculated values

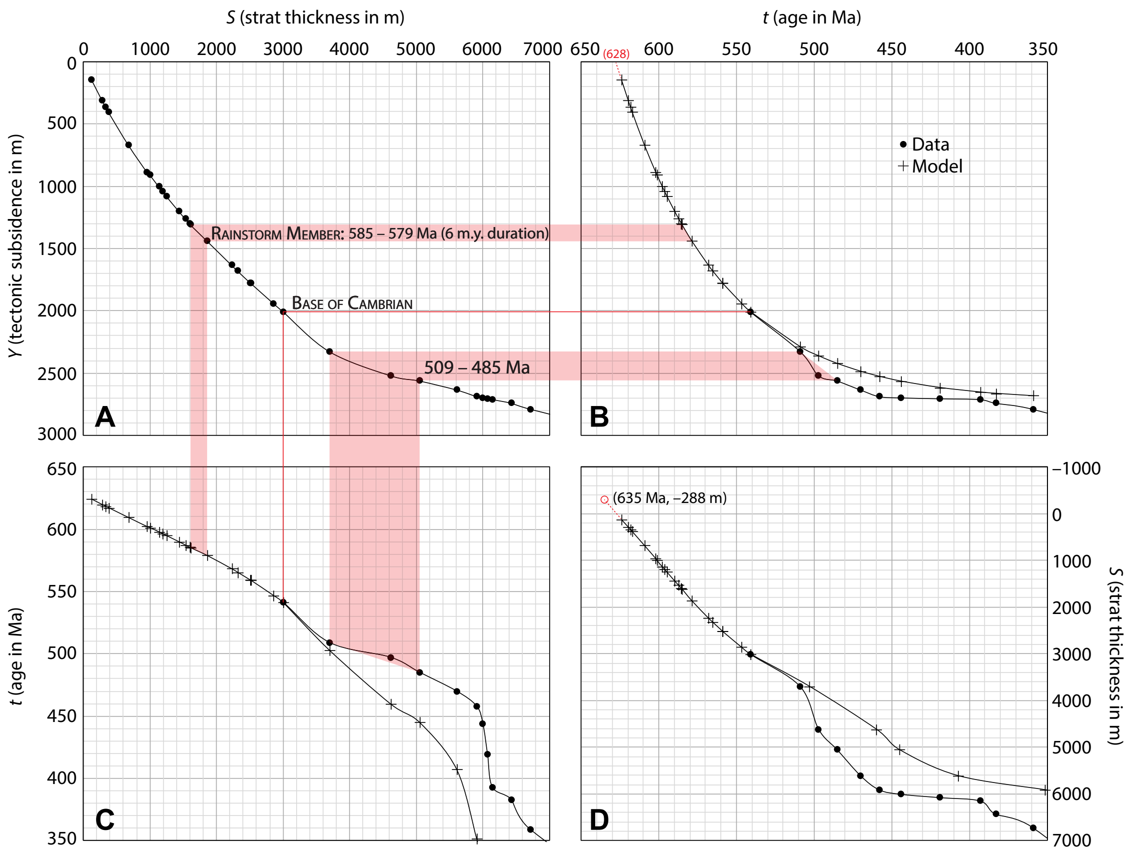

Figure 18. Plots showing subsidence data and model for northwest Spring Mountains section of southwest Laurentia: (A) observed subsidence (stratigraphic thickness) (*S*) vs. tectonic subsidence (*Y*); (B) temporal control on *Y* vs. time applied to Cambrian and younger points (solid circles), where temporal model is shown with plus symbols; (C) similar to B, except showing *S* vs. *t*; and (D) same as C but with axes inverted. Dotted red line and number in B show projected age of the base of Johnnie unit A; dotted red line and circle in D show the amount of additional, hypothetical strata that would be needed below unit A in the Spring Mountains in order for sedimentation to extend linearly back in time to 635 Ma.

of τ for values of tectonic subsidence Y in a series of models that encompass these parameter variations (Table 5). In addition, we defined Y according to two different assumptions for the point at which mechanical stretching ends and purely thermal subsidence begins, where $Y = 0$ (i.e., $e = E_0r$). One is at the lowest exposed stratum (base of unit A), and the other is within unit C, above the youngest ball-and-pillow structure at the top of unit B, assuming seismic shaking ended near this point. In Table 5, models with no Pahrump Group substrate are designated Y_{ns}, and those that include the substrate are designated Y_{ws}; intermediate-density models contain no additional subscript, and low- and high-density models are also subscripted "low" and "high," respectively. Models with "**" define $Y = 0$ within unit C, and models with no superscript assume $Y = 0$ at the base of unit A. We defined the value of Y for which $e = 0$ to be the average of Y(393 Ma) and Y(383 Ma), designated Y(c. 388) in Table 5. The results are insensitive to this choice because there is so little variation in Y between 444 and 383 Ma. We cannot choose the next younger point in the subsidence profile (359 Ma), because it clearly reflects the onset of subsidence associated with Antler foredeep sedimentation.

The contrast in τ between models Y_{ns} and Y_{ws} is only 3 m.y., with $\tau = 55$ and 52 m.y., respectively. As expected from Equation 4, the definition point of $Y = 0$ has no effect, because we define e_1 and e_2 on the basis of differences in Y values late in the subsidence history. For models with no substrate, varying the density between $Y_{ns,\,low}$ and $Y_{ns,\,high}$ (corresponding to the assumption of high and low sediment grain density, respectively) has a substantial effect on τ, which ranges from 42 to 65 m.y., respectively. For models $Y_{ws,\,low}$ to $Y_{ws,\,high}$, the sensitivity is even greater, with τ varying from 36 to 63 m.y., respectively. Clearly, the upper part of these ranges accords with subsidence patterns in Mesozoic and Cenozoic basins. Despite the nearly 30 m.y. variation in τ among these models, we note that there is relatively little variation in the modeled age and duration of the Shuram excursion (Table 5). Among this suite of models, the onset varies by 12 m.y. (from 569 to 581 Ma), the

TABLE 5. ESTIMATES FOR THE TIME CONSTANT τ[†]

Model	Y(541)	Y(509)	Y(393)	Y(383)	Y(c. 388)[§]	τ (m.y.)	SE begin[#] (Ma)	SE end[#] (Ma)
Y_{ns}	2009	2327	2713	2743	2728	55	578	573
Y_{ns}**	1646	1964	2350	2380	2365	55	578	573
Y_{ws}	2757	3029	3334	3358	3346	52	575	570
$Y_{ns, low}$	1844	2125	2367	2380	2374	42	574	569
Y_{ns}	2009	2327	2713	2743	2728	55	578	573
$Y_{ns, high}$	2173	2528	3058	3105	3082	65	581	575
$Y_{ns, low}$**	1500	1781	2023	2036	2030	42	574	569
Y_{ns}**	1646	1964	2350	2380	2365	55	578	573
$Y_{ns, high}$**	1791	2146	2676	2723	2700	65	581	575
$Y_{ws, low}$	2475	2710	2871	2878	2875	36	569	566
Y_{ws}	2757	3029	3334	3358	3346	52	575	570
$Y_{ws, high}$	3037	3347	3795	3836	3816	63	578	573

[†]Units for τ are millions of years (m.y.). Units for all *Y* values are in meters (m).
[§]Mean value of *Y*(393 Ma) and *Y*(383 Ma).
[#]SE—Shuram excursion.
***Y* values were adjusted by assuming a zero datum that represents a specific point in the stratigraphic column inferred to represent cessation of mechanical stretching and inception of passive-margin thermal subsidence.

termination varies by 9 m.y. (from 566 to 575 Ma), and the duration varies by 3 m.y. (from 3 to 6 m.y.).

A further consideration in estimating τ is the fact that because the Sauk transgression was well under way by 509 Ma, relative sea level may have been slightly higher than at 541 Ma. To the extent that it was, a significant systematic error is introduced in our estimate of τ. For example, for the model with no substrate and intermediate density, a correction in *Y*(509) of just –50 m to account for a change in sea level (+50 m in e_2) changes the estimate of τ from 55 to 69 m.y. (Eq. 1 *in* Steckler and Watts, 1978; Eq. 4 herein). Thus, although the suite of models used for our sensitivity analysis may suggest an estimate of 50 ± ~15 m.y. for τ, the systematic error introduced by the Sauk transgression, and the range of values indicated by models of Mesozoic and Cenozoic basins both suggest a value toward the upper end of this range. We further note that the earliest empirical fits to long-term seafloor subsidence data suggested a value of 62.8 m.y. (Eq. 22 *in* Parsons and Sclater, 1977; table 1 *in* McKenzie, 1978).

Based on these considerations, we developed a second suite of models for estimating pre–541 Ma ages of various horizons within the Johnnie Formation. For this suite, we chose a "midrange" model using what are perhaps the simplest set of assumptions: (1) intermediate sediment grain density values; (2) negligible Pahrump Group substrate; and (3) a time constant of τ = 65 m.y. Using these assumptions, we tied the subsidence curve to the oldest dated point at 541 Ma, minimizing both the amount of extrapolation back in time, and the degree to which the data reflect sea-level rise due to the Sauk and subsequent cratonic flooding events. The resulting subsidence model for the Spring Mountains section is shown in Figure 18 and in Table 6 in the second column from the right-hand side. The remaining columns in Table 6 and Table S2 (footnote 1) demonstrate the sensitivity of our resulting age estimates for the Shuram excursion and other horizons in the Johnnie and Stirling formations to variations in density, τ, and the presence or absence of a substrate. Varying only sediment grain density, limits on the Shuram excursion (tops of units Zjr1 to Zjr2) are 581–575 Ma (low-density case), 585–579 Ma (intermediate density), and 592–585 Ma (high density; Fig. S4 [footnote 1]). Thus, we see that the end of the Shuram excursion varies from 575 to 585 Ma, a range that is centered on the timing of the Gaskiers glaciation. We also note that the duration of the excursion is 6–7 m.y., and it is therefore insensitive to variations in sediment grain density. With regard to sensitivity to the time constant, the end of the Shuram excursion for intermediate density values is 579, 576, and 573 Ma for τ = 65, 60, and 55 m.y., respectively (Fig. S5 [footnote 1]). In terms of the error introduced by the presence of a Pahrump Group substrate (Fig. S6; Table S2 [footnote 1]), for τ = 65 m.y. and intermediate values of density, the Shuram excursion occurs from 584 to 578 Ma, which is only 1 m.y. later than, and of the same duration as, the case of no substrate. The duration of the Shuram excursion across all models in this suite ranges from 4 to 7 m.y. If we exclude with-substrate models (Table S2 [footnote 1]), the variation decreases to 5–7 m.y., and if we further restrict the time constant to 65 m.y., it decreases to 6–7 m.y. These estimates are consistent with recent estimates of 8–9 m.y. for the Johnnie Formation, South Australia (Wonoka), and central China (Doushantuo) sections, based on rock magnetic chronostratigraphy (Minguez et al., 2015; Minguez and Kodama, 2017; Gong et al., 2017). These estimates are all considerably shorter than the subsidence-based estimate of 50 m.y. for the Shuram excursion in Oman (Le Guerroué et al., 2006b), which has been called

TABLE 6. ALL AGES MODELED USING NO SUBSTRATE

		Model ages (Ma)								
		τ = 55 m.y.			τ = 60 m.y.			τ = 65 m.y.		
Unit	Age† (Ma)	Min	Int	Max	Min	Int	Max	Min	Int	Max
MzPzco	Ca. 243	–	–	–	–	–	–	–	–	–
Ddg	359	–	–	–	–	–	–	–	–	–
Dn	383	–	–	–	–	–	–	–	–	–
Dl	393	341	328	303	323	309	281	305	289	260
Sl	419	363	349	323	347	332	303	331	314	283
Oes	444	378	364	337	363	348	319	348	332	300
Oe	458	393	381	352	380	366	335	366	352	317
Op1	470	435	428	415	425	418	404	416	407	393
OЄn1	485	467	460	446	460	452	437	453	445	429
Єbk1	497	481	472	455	475	466	447	470	460	439
Єc1	509	514	509	499	511	506	496	509	503	492
ЄZwc1	541	541	541	541	541	541	541	541	541	541
Zse	–	545	546	547	546	546	547	546	547	548
Zsd	–	555	556	559	556	558	560	557	559	562
Zsc	–	555	556	559	556	558	561	557	559	562
Zsb	–	560	562	565	561	563	567	563	565	569
Zsa	–	562	564	568	564	566	570	565	568	573
Zjr2	–	570	573	578	573	576	581	575	579	585
Zjr1	–	575	578	584	578	582	588	581	585	592
Zjl	–	575	579	584	578	582	588	581	586	592
Zjk	–	576	580	586	580	584	590	583	587	594
Zjj	–	579	582	588	582	586	592	585	590	597
Zji	–	582	587	593	586	591	598	590	595	602
Zjh	–	584	588	594	587	592	599	591	596	604
Zjg	–	585	589	596	589	593	601	593	598	606
Zjf	–	588	592	599	592	597	604	596	601	610
Zje	–	588	593	600	592	597	605	597	602	610
Zjd	–	594	599	606	599	604	612	603	609	618
Zjc2	–	600	605	614	605	611	620	611	617	627
Zjc1	–	601	606	615	606	612	622	612	618	628
Zjb	–	602	608	616	607	614	623	613	620	630
Zja	–	605	611	620	611	618	627	617	624	635
(base)	–	608	614	623	614	621	631	620	628	639

†Ages are at top of unit.

into question on the basis that the Khufai/Shuram interval was probably not deposited on a thermally subsiding continental shelf (Bowring et al., 2007).

In sum, because the timing of the Shuram excursion is within ~0.5τ of 541 Ma, varying parameters in the exponential subsidence model yields variations in our estimate of age and duration of the Shuram excursion of just a few million years. The fact that a fairly broad range of parameters leads to estimates of the end of the Shuram excursion centered on 579 Ma suggests that the valleys incised into the Rainstorm Member are indeed a manifestation of the Gaskiers glaciation at equatorial latitudes. To conclude otherwise strains credulity, because Johnnie/Stirling sequence architecture is relatively uneventful for 400–500 m both above and below the Rainstorm Member (Stirling Member A/B and Johnnie units H through L, respectively). If incision was unrelated to the Gaskiers glaciation, this requires: (1) that the most dramatic stratigraphic event in the Johnnie/Stirling interval was close in time, but unrelated to, glaciation; and (2) that the Gaskiers glaciation itself had virtually no impact on the section. In essence, the subsidence analysis provides a relatively coarse estimate of age that "registers" the section with possible correlatives elsewhere. The detailed stratigraphy then fine tunes the age estimate based on a specific correlation with well-dated events elsewhere, in this case, shelf-incision and the Gaskiers glaciation.

The overall consistency of exponential subsidence models with the hypothesis that incision of the Rainstorm Member shelf is an expression of the Gaskiers glaciation suggests that modeled ages of other horizons in the Johnnie/Stirling interval may also be accurate to within a few million years. The overall accuracy of this model can be further tested by assessing how well it estimates the age of the lowermost Johnnie and Noonday interval. As noted above in our discussion of the possible correlation of unit A with the Noonday Formation, we would expect the age of this unit to be close to the age of the base of the Noonday Formation, or 635 Ma (Petterson et al., 2011). The ranges of modeled ages for the base of unit A are 639–608 Ma (Table 6), with the "midrange" model shown in Figure 18B predicting an age of 628 Ma. As shown in Figure 18D, linear extrapolation below the deepest exposed strata of unit A, assuming a linear deposition rate, would require only an additional 288 m of "subunit A" strata to bring the section to the base of the Noonday Formation and the Ediacaran Period. This thickness plus the 125 m thickness of unit A yields a total thickness of 413 m, which is consistent with maximum known thicknesses of the Noonday Formation (Petterson et al., 2011). The apparent success of exponential subsidence models in predicting the age of both the Gaskiers event and the base of the Ediacaran Period at their most likely stratigraphic levels supports the hypothesis that Ediacaran deposition on the southwest Laurentian margin was largely continuous, and that the Noonday through Wood Canyon interval in its thickest, most basinal exposures does not contain unconformities with significant depositional hiatuses.

CONCLUSIONS

Lithostratigraphic and chemostratigraphic details of the Johnnie Formation at its type locality in the northwest Spring Mountains of southern Nevada provide a basis for regional lithostratigraphic correlation, global chemostratigraphic correlation, and subsidence analysis of the southwest Laurentian continental margin. The regional lithostratigraphy of Ediacaran through Cambrian Age 4 strata defines seven sand-rich intervals separated by siltstone- and carbonate-rich intervals, the upper two of which are the Sauk I and Sauk II sequences of Cambrian age (Palmer, 1981). The great overall thickness of the Johnnie Formation at its type locality (~1800 m), and the apparent absence of subaerial exposure surfaces or other evidence of erosion that are well expressed in more cratonic sections, such as the Nopah Range section, support the hypothesis of continuous deposition. Nonetheless, the lithostratigraphy is strongly cyclic at the kilometer scale, suggesting that significant hiatuses, or at least greatly reduced rates of sediment flux, may be associated with the base of each of the seven sand-rich intervals, even in the more basinal sections. We therefore caution that the true slope of the observed sediment accumulation curve $S(t)$ is almost certainly more variable than that shown in Figure 18D, especially for the segment between 635 Ma and 541 Ma. This concern is tempered by the fact that sediment flux was sufficient in Ediacaran and Paleozoic time to fill the accommodation space to within a few meters to a few tens of meters of sea level, implying that the tectonic component of subsidence was fully recorded.

Carbon isotopic data from sub–Rainstorm Member (sub–Shuram excursion) units in the Mount Schader section are generally positive and support correlation of Johnnie Formation units H through L with the Khufai Formation in Oman, but they do not require it. If correlative, the Mount Schader section would provide the first confirmation of an extended period (represented by 300–400 m of section) of positive $\delta^{13}C$ values prior to the Shuram excursion in both Oman and Nevada.

The Gaskiers glaciation marks the beginning of widespread preservation of macroscopic Ediacaran animals (Xiao et al., 2016), and the Shuram excursion is the largest known carbon isotopic excursion in the geological record. A central issue in animal evolution is thus whether or not the Shuram excursion was approximately synchronous with the Gaskiers event, because it suggests that the Shuram excursion, whatever its cause, was genetically related to creating a surface environment that could support the metabolic requirements of macroscopic animals. A second consequence of Shuram-Gaskiers correlation is that it places the transition from diverse, ornamented acritarchs to a lower-diversity, unornamented assemblage in synchronism with the appearance of macroscopic animals, rather than at some later time. The issue is addressable in southwest Laurentia, to the extent that deposition of Johnnie Formation and related strata occurred more-or-less continuously on a thermally subsiding passive margin.

Based on this assumption, subsidence analysis strongly suggests that the end of Johnnie Formation deposition, at the time of valley incision and subsequent fill with the conglomeratic member, was correlative with the Gaskiers glaciation at 579 Ma. The analysis also suggests that the onset of the Shuram excursion near the base of the Rainstorm Member occurred at ca. 585 Ma. The implied 6 m.y. duration of the Shuram excursion is consistent with paleomagnetic and other proxies from sections in Laurentia and Australia. The subsidence analysis further indicates that if the assignment of the Gaskiers event to uppermost Johnnie time is correct, then the base of the Johnnie Formation is ca. 630 Ma. If so, then the Johnnie through lower Wood Canyon interval in the Spring Mountains represents a relatively complete, 3000-m-thick section that records most or all of Ediacaran time.

ACKNOWLEDGMENTS

We are grateful to Gillian Anderson, Leah Sabbeth, Fenfang Wu, and the late Lindsey Hedges for assistance in the field and laboratory, and to Associate Editor Christopher J. Spencer and reviewer Tony Prave for insightful and constructive reviews. This material is based upon work supported by the National Science Foundation Graduate Research Fellowship Program under grant 1144469 awarded to R. Witkosky, and grant EAR 14-51055 awarded to B. Wernicke.

APPENDIX. DESCRIPTION OF MAP UNITS

Descriptions apply to geologic maps and stratigraphic columns shown in Figures 3, 4, 6, and 7.

Qa: Alluvium and colluvium in active/ephemeral channels and piedmont-forming slopes.

QTl: In Johnnie Wash, a topographically prominent ridge of coarse, poorly sorted debris, here interpreted as a landslide deposit.

Zsa: Stirling Formation, A Member (labeled "Zs" on maps). Very pale-orange, grayish-black–weathering, medium-grained orthoquartzite, laminated to massive, medium to thick bedded, with trough cross-stratification. Contains some interbedded carbonate-cemented sandstone. In places, bedding is destroyed by secondary brecciation and recementation, forming irregular dark-weathering masses. Unit forms resistant ridges relative to underlying Johnnie Formation.

Zjr: Johnnie Formation, Rainstorm Member. Includes four distinct subunits, from bottom to top: (1) green phyllitic siltstone, (2) highly resistant, ocher-colored oolitic dolostone ("Johnnie oolite," indicated by red open-dotted line, ~2 m thick), (3) pale-red, carbonate-cemented, fine-grained sandstone and sandy limestone, and (4) a heterogeneous upper unit that includes siltstone, carbonate-rich sandstone, flaser-bedded sandy carbonate, and intraformational limestone breccia. In the Mount Schader section, an ~4-m-thick triad of orthoquartzite, siltstone, and dolostone immediately underlies the Stirling Formation. Orthoquartzite is affected by meter-scale ball-and-pillow structure.

Zjl: Orthoquartzite and variegated siltstone. Generally a recessive/slope-forming unit. Red dotted line on Mount Schader map indicates a resistant, laminated, brown dolomitic marker bed, ~2 m thick.

Zjk: Orthoquartzite, variegated siltstone, and dolostone. Orthoquartzite is parallel bedded and forms erosionally resistant base; siltstone locally contains ripple laminations; resistant, brown, dolomitic marker bed, indicated by red dotted line in Mount Schader map area, is hummocky cross-stratified and contains chert in its lower portion.

Zjj: Orthoquartzite, variegated siltstone, and minor dolomitic sandstone. Orthoquartzite and siltstone occur in ~5 m cycles. Orthoquartzite is white, resistant, and locally granular, and it contains high-angle (~20°) cross-stratification; dolomitic sandstones are thick, brown, resistant, fine- to medium-grained beds. Red dotted line on both maps indicates a hummocky cross-stratified, brown dolomite marker bed.

Zji: Orthoquartzite, variegated siltstone, and dolomitic sandstone, parallel bedded in the Johnnie Wash section, and hummocky cross-stratified in the Mount Schader section. Orthoquartzite is fine-grained and occurs as conspicuous thick-bedded intervals in 5–10 m cycles with siltstones. Red dotted line on Mount Schader map indicates a hummocky cross-stratified, brown dolomitic sandstone marker bed.

Zjh: Orthoquartzite and variegated siltstone. Red dotted lines on Mount Schader map indicate brown, hummocky cross-stratified dolomite marker beds that contain stromatolitic mounds.

Zjg: Variegated fine-grained sandstone and siltstone, weakly cemented; also occasional interstratified orthoquartzite, fine to medium grained, medium to thick bedded.

Zjf: Dolostone with centimeter- to decimeter-thick, centimeter- to meter-long chert nodules and lenses. The dolostone forms a conspicuous pale-weathering ridge. It is finely laminated to massive. Microcrystalline varieties weather gray; coarser-grained, secondary dolomite weathers dark gray to brown.

Zje: Massive, fine-grained sandstone and laminated siltstone. Upper part contains several dozen rhythmic cycles, ~2 m thick, of sandstone and siltstone. Each cycle has a sharp, load-casted bottom and grades upward from sandstone to siltstone. Generally an olive-hued, recessive/slope-forming unit, with occasional beds of cross-stratified sandstone, similar to unit D.

Zjd: Well-cemented, fine-grained orthoquartzite in meter-scale beds featuring cross-stratification with steep truncation angles (up to ~30°), interstratified with medium-grained, weakly hematite-cemented ferruginous sandstone and variegated siltstone. Unit forms resistant ridge that is conspicuously darker weathering than unit E.

Zjc: Siltstone (as Zja) with a calcareous, medium-grained orthoquartzite marker bed, similar to unit D, indicated on Figure 3 by green dotted line. The lowest carbonate in the Johnnie Wash section appears near the top of this unit as a brown, medium-grained, fabric-retentive dolostone.

Zjb: Interstratified fine-grained orthoquartzite and phyllitic siltstone. Orthoquartzite occurs in meter-scale beds with parallel lamination, pervasively disrupted by soft sediment deformation, primarily ball-and-pillow structure, such that individual beds are difficult to trace along strike.

Zja: Phyllitic siltstone, with a distinct crenulation cleavage at high angle to bedding, generally a recessive unit.

REFERENCES CITED

Abolins, M.J., 1999, I. Stratigraphic Constraints on the Number of Discrete Neoproterozoic Glaciations and the Relationship between Glaciation and Ediacaran Evolution; II. The Kwichup Spring Thrust in the Northwest Spring Mountains, Nevada: Implications for Large-Magnitude Extension and the Structure of the Cordilleran Thrust Belt [Ph.D. thesis]: Pasadena, California, California Institute of Technology, 341 p.

Abolins, M., Oskin, R., Prave, T., Summa, C., and Corsetti, F., 2000, Neoproterozoic glacial record in the Death Valley region, California and Nevada, *in* Lageson, D.R., Peters, S.G., and Lahren, M.M., eds., Great Basin and Sierra Nevada: Geological Society of America Field Guide 2, p. 319–335, https://doi.org/10.1130/0-8137-0002-7.319.

Albee, A.L., Labotka, T.C., Lanphere, M.A., and McDowell, S.D., 1981, Geologic Map of the Telescope Peak Quadrangle, California: U.S. Geological Survey Geological Quadrangle Map GQ-1532, scale 1:62,500, 1 sheet.

Alfaro, P., Delgado, J., Estévez, A., Molina, J.M., Moretti, M., and Soria, J.M., 2002, Liquefaction and fluidization structures in Messinian storm deposits (Bajo Segura Basin, Betic Cordillera, southern Spain): International Journal of Earth Sciences, v. 91, p. 505–513, https://doi.org/10.1007/s00531-001-0241-z.

Allan, J.R., and Matthews, R.K., 1977, Carbon and oxygen isotopes as diagenetic and stratigraphic tools: Surface and subsurface data, Barbados, West Indies: Geology, v. 5, p. 16–20, https://doi.org/10.1130/0091-7613(1977)5<16:CAOIAD>2.0.CO;2.

Allan, J.R., and Matthews, R.K., 1982, Isotope signatures associated with early meteoric diagenesis: Sedimentology, v. 29, p. 797–817, https://doi.org/10.1111/j.1365-3091.1982.tb00085.x.

Allen, P.A., and Allen, J.R., 2005, Basin Analysis: Principles and Applications (second edition): Malden, Massachusetts, Blackwell Publishing, 549 p.

Allmendinger, R.W., Cardozo, N., and Fisher, D., 2012, Structural Geology Algorithms: Vectors and Tensors in Structural Geology: Cambridge, UK, Cambridge University Press, 302 p.

Armin, R.A., and Mayer, L., 1983, Subsidence analysis of the Cordilleran miogeocline: Implications for timing of late Proterozoic rifting and amount of extension: Geology, v. 11, p. 702–705, https://doi.org/10.1130/0091-7613(1983)11<702:SAOTCM>2.0.CO;2.

Bekker, A., and Holland, H.D., 2012, Oxygen overshoot and recovery during the early Paleoproterozoic: Earth and Planetary Science Letters, v. 317–318, p. 295–304, https://doi.org/10.1016/j.epsl.2011.12.012.

Benmore, W.C., 1978, Stratigraphy, Sedimentology, and Paleoecology of the Late Paleophytic or Earliest Phanerozoic Johnnie Formation, Eastern California and Southwestern Nevada [Ph.D. thesis]: Santa Barbara, California, University of California, 243 p.

Bergmann, K.D., Zentmyer, R.A., and Fischer, W.W., 2011, The stratigraphic expression of a large negative carbon isotope excursion from the Ediacaran Johnnie Formation, Death Valley: Precambrian Research, v. 188, p. 45–56, https://doi.org/10.1016/j.precamres.2011.03.014.

Boggs, S., Jr., 2012, Principles of Sedimentology and Stratigraphy (5th ed.): Englewood Cliffs, New Jersey, Pearson Prentice Hall, 585 p.

Bond, G.C., and Kominz, M.A., 1984, Construction of tectonic subsidence curves for the early Paleozoic miogeocline, southern Canadian Rocky Mountains: Implications for subsidence mechanisms, age of breakup, and crustal thinning: Geological Society of America Bulletin, v. 95, no. 2, p. 155–173, https://doi.org/10.1130/0016-7606(1984)95<155:COTSCF>2.0.CO;2.

Bond, G.C., Kominz, M.A., and Devlin, W.J., 1983, Thermal subsidence and eustasy in the Lower Palaeozoic miogeocline of western North America: Nature, v. 306, no. 5945, p. 775–779, https://doi.org/10.1038/306775a0.

Bond, G.C., Kominz, M.A., and Grotzinger, J.P., 1988, Cambro-Ordovician eustasy: Evidence from geophysical modelling of subsidence in Cordilleran and Appalachian passive margins, *in* Kleinspehn, K.L., and Paola, C., eds., New Perspectives in Basin Analysis: New York, Springer, p. 129–160, https://doi.org/10.1007/978-1-4612-3788-4_7.

Bowring, S., Myrow, P., Landing, E., Ramezani, J., Condon, D., and Hoffmann, K.H., 2003a, Geochronological constraints on Neoproterozoic glaciations and the rise of metazoans: Geological Society of America Abstracts with Programs, v. 35, no. 6, p. 516.

Bowring, S.A., Myrow, P.M., Landing, E., and Ramezani, J., 2003b, Geochronological constraints on terminal Neoproterozoic events and the rise of metazoans: Geophysical Research Abstracts, v. 5, no. 13219, p. 219.

Bowring, S.A., Grotzinger, J.P., Condon, D.J., Ramezani, J., Newall, M.J., and Allen, P.A., 2007, Geochronologic constraints on the chronostratigraphic framework of the Neoproterozoic Huqf Supergroup, Sultanate of Oman: American Journal of Science, v. 307, p. 1097–1145, https://doi.org/10.2475/10.2007.01.

Burchfiel, B.C., 1964, Precambrian and Paleozoic stratigraphy of Specter Range quadrangle, Nye County, Nevada: American Association of Petroleum Geologists Bulletin, v. 48, no. 1, p. 40–56.

Burchfiel, B.C., 1965, Structural geology of the Specter Range quadrangle, Nevada, and its regional significance: Geological Society of America Bulletin, v. 76, no. 2, p. 175–192, https://doi.org/10.1130/0016-7606(1965)76[175:SGOTSR]2.0.CO;2.

Burchfiel, B.C., and Davis, G.A., 1972, Structural framework and evolution of the southern part of the Cordilleran orogen, western United States: American Journal of Science, v. 272, no. 2, p. 97–118, https://doi.org/10.2475/ajs.272.2.97.

Burchfiel, B.C., and Davis, G.A., 1975, Nature and controls of Cordilleran orogenesis, western United States: Extensions of an earlier synthesis: American Journal of Science, v. 275-A, p. 363–396.

Burchfiel, B.C., Fleck, R.J., Secor, D.T., Vincelette, R.R., and Davis, G.A., 1974, Geology of the Spring Mountains, Nevada: Geological Society of America Bulletin, v. 85, p. 1013–1022, https://doi.org/10.1130/0016-7606(1974)85<1013:GOTSMN>2.0.CO;2.

Burchfiel, B.C., Hamill, G.S., IV, and Wilhelms, D.E., 1983, Structural geology of the Montgomery Mountains and the northern half of the Nopah and Resting Spring Ranges, Nevada and California: Geological Society of America Bulletin, v. 94, p. 1359–1376, https://doi.org/10.1130/0016-7606(1983)94<1359:SGOTMM>2.0.CO;2.

Burns, S.J., and Matter, A., 1993, Carbon isotopic record of the latest Proterozoic from Oman: Eclogae Geologicae Helvetiae, v. 86, no. 2, p. 595–607.

Butterfield, N.J., 2009, Oxygen, animals, and oceanic ventilation: An alternative view: Geobiology, v. 7, p. 1–7, https://doi.org/10.1111/j.1472-4669.2009.00188.x.

Calver, C.R., 2000, Isotope stratigraphy of the Ediacaran (Neoproterozoic III) of the Adelaide Rift Complex, Australia, and the overprint of water column stratification: Precambrian Research, v. 100, p. 121–150, https://doi.org/10.1016/S0301-9268(99)00072-8.

Canfield, D.E., Poulton, S.W., and Narbonne, G.M., 2007, Late Neoproterozoic deep-ocean oxygenation and the rise of animal life: Science, v. 315, no. 5808, p. 92–95, https://doi.org/10.1126/science.1135013.

Cardozo, N., 2009, Backstrip: http://www.ux.uis.no/~nestor/work/programs.html (accessed August 2017).

Cardozo, N., and Allmendinger, R.W., 2013, Spherical projections with OSXStereonet: Computers & Geosciences, v. 51, p. 193–205, https://doi.org/10.1016/j.cageo.2012.07.021.

Clapham, M.E., and Corsetti, F.A., 2005, Deep valley incision in the terminal Neoproterozoic (Ediacaran) Johnnie Formation, eastern California, USA: Tectonically or glacially driven?: Precambrian Research, v. 141, p. 154–164, https://doi.org/10.1016/j.precamres.2005.09.002.

Cohen, P.A., Bradley, A., Knoll, A.H., Grotzinger, J.P., Jensen, S., Abelson, J., Hand, K., Love, G., Metz, J., McLoughlin, N., Meister, P., Shepard, R., Tice, M., and Wilson, J.P., 2009, Tubular compression fossils from the Ediacaran Nama Group, Namibia: Journal of Paleontology, v. 83, p. 110–122, https://doi.org/10.1017/S0022336000058169.

Condon, D., Zhu, M., Bowring, S., Wang, W., Yang, A., and Jin, Y., 2005, U-Pb ages from the Neoproterozoic Doushantuo Formation, China: Science, v. 308, p. 95–98, https://doi.org/10.1126/science.1107765.

Corsetti, F.A., and Hagadorn, J.W., 2000, Precambrian-Cambrian transition: Death Valley, United States: Geology, v. 28, no. 4, p. 299–302, https://doi.org/10.1130/0091-7613(2000)28<299:PTDVUS>2.0.CO;2.

Corsetti, F.A., and Kaufman, A.J., 2003, Stratigraphic investigations of carbon isotope anomalies and Neoproterozoic ice ages in Death Valley, California: Geological Society of America Bulletin, v. 115, no. 8, p. 916–932, https://doi.org/10.1130/B25066.1.

Corsetti, F.A., Awramik, S.M., Pierce, D., and Kaufman, A.J., 2000, Using chemostratigraphy to correlate and calibrate unconformities in Neoproterozoic strata from the southern Great Basin of the United States: International Geology Review, v. 42, p. 516–533, https://doi.org/10.1080/00206810009465096.

Deer, W.A., Howie, R.A., and Zussman, J., 1992, An Introduction to the Rock-Forming Minerals (2nd ed.): London, UK, Pearson Education Limited, 696 p.

Derry, L.A., 2010a, A burial diagenesis origin for the Ediacaran Shuram-Wonoka carbon isotope anomaly: Earth and Planetary Science Letters, v. 294, no. 1–2, p. 152–162, https://doi.org/10.1016/j.epsl.2010.03.022.

Derry, L.A., 2010b, On the significance of $\delta^{13}C$ correlations in ancient sediments: Earth and Planetary Science Letters, v. 296, p. 497–501, https://doi.org/10.1016/j.epsl.2010.05.035.

Dickinson, W.R., 1977, Paleozoic plate tectonics and the evolution of the Cordilleran continental margin, *in* Stewart, J.H., Stevens, C.H., and Fritsche, A.E., eds., Paleozoic Paleogeography of the Western United States: Los Angeles, California, Pacific Section, Society of Economic Paleontologists and Mineralogists (SEPM), Pacific Coast Paleogeography Symposium 1, p. 137–156.

Fedo, C.M., and Cooper, J.D., 2001, Sedimentology and sequence stratigraphy of Neoproterozoic and Cambrian units across a craton-margin hinge zone, southeastern California, and implications for the early evolution of the Cordilleran margin: Sedimentary Geology, v. 141–142, p. 501–522, https://doi.org/10.1016/S0037-0738(01)00088-4.

Field, C.B., Behrenfeld, M.J., Randerson, J.T., and Falkowski, P., 1998, Primary production of the biosphere: Integrating terrestrial and oceanic components: Science, v. 281, p. 237–240, https://doi.org/10.1126/science.281.5374.237.

Fike, D.A., Grotzinger, J.P., Pratt, L.M., and Summons, R.E., 2006, Oxidation of the Ediacaran ocean: Nature, v. 444, p. 744–747, https://doi.org/10.1038/nature05345.

Gabrielse, H., 1972, Younger Precambrian of the Canadian Cordillera: American Journal of Science, v. 272, no. 6, p. 521–536, https://doi.org/10.2475/ajs.272.6.521.

Giallorenzo, M.A., Wells, M.L., Yonkee, W.A., Stockli, D.F., and Wernicke, B.P., 2017, Timing of exhumation, Wheeler Pass thrust sheet, southern Nevada and California: Late Jurassic to middle Cretaceous evolution of the southern Sevier fold-and-thrust belt: Geological Society of America Bulletin, v. 130, no. 3–4, p. 558–579, https://doi.org/10.1130/B31777.1.

Gillett, S.L., and Van Alstine, D.R., 1982, Remagnetization and tectonic rotation of Upper Precambrian and Lower Paleozoic strata from the Desert Range, southern Nevada: Journal of Geophysical Research, v. 87, no. B13, p. 10,929–10,953, https://doi.org/10.1029/JB087iB13p10929.

Gong, Z., Kodama, K.P., and Li, Y.-X., 2017, Rock magnetic cyclostratigraphy of the Doushantuo Formation, South China, and its implications for the duration of the Shuram carbon isotope excursion: Precambrian Research, v. 289, p. 62–74, https://doi.org/10.1016/j.precamres.2016.12.002.

Grotzinger, J.P., Fike, D.A., and Fischer, W.W., 2011, Enigmatic origin of the largest-known carbon isotope excursion in Earth's history: Nature Geoscience, v. 4, no. 5, p. 285–292, https://doi.org/10.1038/ngeo1138.

Hagadorn, J.W., and Waggoner, B., 2000, Ediacaran fossils from the southwestern Great Basin, United States: Journal of Paleontology, v. 74, no. 2, p. 349–359, https://doi.org/10.1017/S0022336000031553.

Halley, R.B., and Schmoker, J.W., 1983, High-porosity Cenozoic carbonate rocks of south Florida: Progressive loss of porosity with depth: American Association of Petroleum Geologists Bulletin, v. 67, no. 2, p. 191–200.

Halverson, G.P., Hoffman, P.F., Schrag, D.P., Maloof, A.C., and Rice, A.H.N., 2005, Toward a Neoproterozoic composite carbon-isotope record: Geological Society of America Bulletin, v. 117, no. 9/10, p. 1181–1207, https://doi.org/10.1130/B25630.1.

Halverson, G.P., Wade, B.P., Hurtgen, M.T., and Barovich, K.M., 2010, Neoproterozoic chemostratigraphy: Precambrian Research, v. 182, p. 337–350, https://doi.org/10.1016/j.precamres.2010.04.007.

Hamill, G.S., IV, 1966, Structure and Stratigraphy of the Mt. Shader Quadrangle, Nye County, Nevada–Inyo County, California [Ph.D. thesis]: Houston, Texas, Rice University, 83 p.

Hazzard, J.C., 1937, Paleozoic section in the Nopah and Resting Springs Mountains, Inyo County, California: California Journal of Mines and Geology, v. 33, no. 4, p. 273–339.

Heaman, L.M., and Grotzinger, J.P., 1992, 1.08 Ga diabase sills in the Pahrump Group, California: Implications for development of the Cordilleran miogeocline: Geology, v. 20, p. 637–640, https://doi.org/10.1130/0091-7613(1992)020<0637:GDSITP>2.3.CO;2.

Hoffman, P.F., Kaufman, A.J., Halverson, G.P., and Schrag, D.P., 1998, A Neoproterozoic Snowball Earth: Science, v. 281, p. 1342–1346, https://doi.org/10.1126/science.281.5381.1342.

Hoffmann, K.-H., Condon, D.J., Bowring, S.A., and Crowley, J.L., 2004, U-Pb zircon date from the Neoproterozoic Ghaub Formation, Namibia: Constraints on Marinoan glaciation: Geology, v. 32, p. 817–820, https://doi.org/10.1130/G20519.1.

Holland, H.D., 2006, The oxygenation of the atmosphere and oceans: Philosophical Transactions of the Royal Society of London, ser. B, Biological Sciences, v. 361, p. 903–915, https://doi.org/10.1098/rstb.2006.1838.

Hollingsworth, J.S., 2005, The earliest occurrence of trilobites and brachiopods in the Cambrian of Laurentia: Palaeogeography, Palaeoclimatology, Palaeoecology, v. 220, p. 153–165, https://doi.org/10.1016/j.palaeo.2004.08.008.

Hunt, D.L., 1990, Trilobite Faunas and Biostratigraphy of the Lower Cambrian Wood Canyon Formation, Death Valley Region, California [Master's thesis]: Davis, California, University of California, 140 p.

Hunter, R.E., 1977, Basic types of stratification in small eolian dunes: Sedimentology, v. 24, no. 3, p. 361–387, https://doi.org/10.1111/j.1365-3091.1977.tb00128.x.

Husson, J.M., Maloof, A.C., Schoene, B., Chen, C.Y., and Higgins, J.A., 2015, Stratigraphic expression of Earth's deepest $\delta^{13}C$ excursion in the Wonoka Formation of South Australia: American Journal of Science, v. 315, p. 1–45, https://doi.org/10.2475/01.2015.01.

Kamb, W.B., 1959, Ice petrofabric observations from Blue Glacier, Washington, in relation to theory and experiment: Journal of Geophysical Research, v. 64, no. 11, p. 1891–1909, https://doi.org/10.1029/JZ064i011p01891.

Kaufman, A.J., Hayes, J.M., Knoll, A.H., and Germs, G.J.B., 1991, Isotopic compositions of carbonates and organic carbon from Upper Proterozoic successions in Namibia: Stratigraphic variation and the effects of diagenesis and metamorphism: Precambrian Research, v. 49, p. 301–327, https://doi.org/10.1016/0301-9268(91)90039-D.

Kaufman, A.J., Corsetti, F.A., and Varni, M.A., 2007, The effect of rising atmospheric oxygen on carbon and sulfur isotope anomalies in the Neoproterozoic Johnnie Formation, Death Valley, USA: Chemical Geology, v. 237, p. 47–63, https://doi.org/10.1016/j.chemgeo.2006.06.023.

Knauth, L.P., and Kennedy, M.J., 2009, The late Precambrian greening of the Earth: Nature, v. 460, no. 7256, p. 728–732, 10.1038/nature08213.

Knoll, A.H., and Carroll, S.B., 1999, Early animal evolution: Emerging views from comparative biology and geology: Science, v. 284, no. 5423, p. 2129–2137, https://doi.org/10.1126/science.284.5423.2129.

Knoll, A.H., Walter, M.R., Narbonne, G.M., and Christie-Blick, N., 2004, A new period for the geologic time scale: Science, v. 305, p. 621–622, https://doi.org/10.1126/science.1098803.

Knoll, A.H., Walter, M.R., Narbonne, G.M., and Christie-Blick, N., 2006, The Ediacaran Period: A new addition to the geologic time scale: Lethaia, v. 39, p. 13–30, https://doi.org/10.1080/00241160500409223.

Kump, L.R., 2008, The rise of atmospheric oxygen: Nature, v. 451, p. 277–278, https://doi.org/10.1038/nature06587.

Labotka, T.C., Albee, A.L., Lanphere, M.A., and McDowell, S.D., 1980, Stratigraphy, structure, and metamorphism in the central Panamint Mountains (Telescope Peak quadrangle), Death Valley area, California: Summary: Geological Society of America Bulletin, v. 91, p. 125–129, https://doi.org/10.1130/0016-7606(1980)91<125:SSAMIT>2.0.CO;2.

Larrieu, T.L., 1995, Basin analysis with a spreadsheet: Journal of Geological Education, v. 43, p. 107–113, https://doi.org/10.5408/0022-1368-43.2.107.

Le Guerroué, E., Allen, P.A., and Cozzi, A., 2006a, Chemostratigraphic and sedimentological framework of the largest negative carbon isotope excursion in Earth history: The Neoproterozoic Shuram Formation (Nafun Group, Oman): Precambrian Research, v. 146, p. 68–92, https://doi.org/10.1016/j.precamres.2006.01.007.

Le Guerroué, E., Allen, P.A., Cozzi, A., Etienne, J.L., and Fanning, M., 2006b, 50 Myr recovery from the largest negative $\delta^{13}C$ excursion in the Ediacaran ocean: Terra Nova, v. 18, p. 147–153, https://doi.org/10.1111/j.1365-3121.2006.00674.x.

Lenton, T.M., Boyle, R.A., Poulton, S.W., Shields-Zhou, G.A., and Butterfield, N.J., 2014, Co-evolution of eukaryotes and ocean oxygenation in the Neoproterozoic Era: Nature Geoscience, v. 7, p. 257–265, https://doi.org/10.1038/ngeo2108.

Levy, M., and Christie-Blick, N., 1991, Tectonic subsidence of the early Paleozoic passive continental margin in eastern California and southern Nevada: Geological Society of America Bulletin, v. 103, p. 1590–1606, https://doi.org/10.1130/0016-7606(1991)103<1590:TSOTEP>2.3.CO;2.

Li, Z.X., et al., 2008, Assembly, configuration, and break-up of Rodinia: A synthesis: Precambrian Research, v. 160, p. 179–210, https://doi.org/10.1016/j.precamres.2007.04.021.

Li, Z.X., Evans, D.A.D., and Halverson, G.P., 2013, Neoproterozoic glaciations in a revised global palaeogeography from the breakup of Rodinia to the assembly of Gondwanaland: Sedimentary Geology, v. 294, p. 219–232, https://doi.org/10.1016/j.sedgeo.2013.05.016.

Longwell, C.R., Pampeyan, E.H., Bowyer, B., and Roberts, R.J., 1965, Geology and Mineral Deposits of Clark County, Nevada: Nevada Bureau of Mines Bulletin 62, 218 p.

Loyd, S.J., Marenco, P.J., Hagadorn, J.W., Lyons, T.W., Kaufman, A.J., Sour-Tovar, F., and Corsetti, F.A., 2012, Sustained low marine sulfate concentrations from the Neoproterozoic to the Cambrian: Insights from carbonates of northwestern Mexico and eastern California: Earth and Planetary Science Letters, v. 339–340, p. 79–94, https://doi.org/10.1016/j.epsl.2012.05.032.

Loyd, S.J., Corsetti, F.A., Eagle, R.A., Hagadorn, J.W., Shen, Y., Zhang, X., Bonifacie, M., and Tripati, A.K., 2015, Evolution of Neoproterozoic Wonoka-Shuram anomaly–aged carbonates: Evidence from clumped isotope paleothermometry: Precambrian Research, v. 264, p. 179–191, https://doi.org/10.1016/j.precamres.2015.04.010.

Macdonald, F.A., Jones, D.S., and Schrag, D.P., 2009, Stratigraphic and tectonic implications of a newly discovered glacial diamictite–cap carbonate couplet in southwestern Mongolia: Geology, v. 37, no. 2, p. 123–126, https://doi.org/10.1130/G24797A.1.

Macdonald, F.A., Strauss, J.V., Sperling, E.A., Halverson, G.P., Narbonne, G.M., Johnston, D.T., Kunzmann, M., Schrag, D.P., and Higgins, J.A., 2013, The stratigraphic relationship between the Shuram carbon isotope excursion, the oxygenation of Neoproterozoic oceans, and the first appearance of the Ediacaran biota and bilaterian trace fossils in northwestern Canada: Chemical Geology, v. 362, p. 250–272, https://doi.org/10.1016/j.chemgeo.2013.05.032.

Mahon, R.C., Dehler, C.M., Link, P.K., Karlstrom, K.E., and Gehrels, G.E., 2014, Geochronologic and stratigraphic constraints on the Mesoproterozoic and Neoproterozoic Pahrump Group, Death Valley, California: A record of the assembly, stability, and breakup of Rodinia: Geological Society of America Bulletin, v. 126, no. 5/6, p. 652–664, https://doi.org/10.1130/B30956.1.

McFadden, K.A., Huang, J., Chu, X., Jiang, G., Kaufman, A.J., Zhou, C., Yuan, X., and Xiao, S., 2008, Pulsed oxidation and biological evolution in the Ediacaran Doushantuo Formation: Proceedings of the National Academy of Sciences of the United States of America, v. 105, no. 9, p. 3197–3202, https://doi.org/10.1073/pnas.0708336105.

McKenzie, D., 1978, Some remarks on the development of sedimentary basins: Earth and Planetary Science Letters, v. 40, p. 25–32, https://doi.org/10.1016/0012-821X(78)90071-7.

McMenamin, M.A.S., 1996, Ediacaran biota from Sonora, Mexico: Proceedings of the National Academy of Sciences of the United States of America, v. 93, p. 4990–4993, https://doi.org/10.1073/pnas.93.10.4990.

Melezhik, V.A., Fallick, A.E., and Pokrovsky, B.G., 2005, Enigmatic nature of thick sedimentary carbonates depleted in ^{13}C beyond the canonical mantle value: The challenges to our understanding of the terrestrial carbon cycle: Precambrian Research, v. 137, p. 131–165, https://doi.org/10.1016/j.precamres.2005.03.010.

Melim, L.A., Swart, P.K., and Maliva, R.G., 1995, Meteoric-like fabrics forming in marine waters: Implications for the use of petrography to identify diagenetic environments: Geology, v. 23, no. 8, p. 755–758, https://doi.org/10.1130/0091-7613(1995)023<0755:MLFFIM>2.3.CO;2.

Melim, L.A., Swart, P.K., and Maliva, R.G., 2001, Meteoric and marine-burial diagenesis in the subsurface of the Great Bahama Bank, *in* Ginsburg, R.N., ed., Subsurface Geology of a Prograding Carbonate Platform Margin, Great Bahama Bank: Results of the Bahamas Drilling Project: Society of Economic Paleontologists and Mineralogists (Society for Sedimentary Geology) Special Publication 70, p. 137–161, https://doi.org/10.2110/pec.01.70.0137.

Minguez, D., and Kodama, K.P., 2017, Rock magnetic chronostratigraphy of the Shuram carbon isotope excursion: Wonoka Formation, Australia: Geology, v. 45, no. 6, p. 567–570, https://doi.org/10.1130/G38572.1.

Minguez, D., Kodama, K.P., and Hillhouse, J.W., 2015, Paleomagnetic and cyclostratigraphic constraints on the synchroneity and duration of the Shuram carbon isotope excursion, Johnnie Formation, Death Valley Region, CA: Precambrian Research, v. 266, p. 395–408, https://doi.org/10.1016/j.precamres.2015.05.033.

Monger, J.W.H., and Price, R.A., 1979, Geodynamic evolution of the Canadian Cordillera—Progress and problems: Canadian Journal of Earth Sciences, v. 16, no. 3, p. 770–791, https://doi.org/10.1139/e79-069.

Myrow, P.M., and Kaufman, A.J., 1999, A newly discovered cap carbonate above Varanger-age glacial deposits in Newfoundland, Canada: Journal of Sedimentary Research, v. 69, no. 3, p. 784–793, https://doi.org/10.2110/jsr.69.784.

Narbonne, G.M., Xiao, S., Shields, G.A., and Gehling, J.G., 2012, The Ediacaran Period, *in* Gradstein, F.M., Ogg, J.G., Schmitz, M., and Ogg, G.M., eds., The Geologic Timescale 2012, Volume 1: Elsevier, p. 207–232, https://doi.org/10.1016/B978-0-444-59425-9.00018-4.

Nolan, T.B., 1924, Geology of the Northwest Portion of the Spring Mountains, Nevada [Ph.D. thesis]: New Haven, Connecticut, Yale University, 125 p.

Nolan, T.B., 1929, Notes on the stratigraphy and structure of the northwest portion of Spring Mountain, Nevada: American Journal of Science, ser. 5, v. 17, no. 101, p. 461–472.

Nursall, J.R., 1959, Oxygen as a prerequisite to the origin of the metazoa: Nature, v. 183, no. 4669, p. 1170–1172, https://doi.org/10.1038/1831170b0.

Och, L.M., and Shields-Zhou, G.A., 2012, The Neoproterozoic oxygenation event: Environmental perturbations and biogeochemical cycling: Earth-Science Reviews, v. 110, p. 26–57, https://doi.org/10.1016/j.earscirev.2011.09.004.

Ogg, J.G., Ogg, G., and Gradstein, F.M., 2016, A Concise Geologic Timescale: 2016: Amsterdam, Netherlands, Elsevier, 240 p.

Osburn, M.R., Owens, J., Bergmann, K.D., Lyons, T.W., and Grotzinger, J.P., 2015, Dynamic changes in sulfate sulfur isotopes preceding the Ediacaran Shuram excursion: Geochimica et Cosmochimica Acta, v. 170, p. 204–224, https://doi.org/10.1016/j.gca.2015.07.039.

Palmer, A.R., 1981, Subdivision of the Sauk sequence, *in* Taylor, M.E., ed., Short Papers for the Second International Symposium on the Cambrian System: U.S. Geological Survey Open-File Report 81–743, p. 160–163.

Palmer, A.R., and Halley, R.B., 1979, Physical Stratigraphy and Trilobite Biostratigraphy of the Carrara Formation (Lower and Middle Cambrian) in the Southern Great Basin: U.S. Geological Survey Professional Paper 1407, 131 p.

Parsons, B., and Sclater, J.G., 1977, An analysis of the variation of ocean floor bathymetry and heat flow with age: Journal of Geophysical Research, v. 82, no. 5, p. 803–827, https://doi.org/10.1029/JB082i005p00803.

Petterson, R., Prave, A.R., Wernicke, B.P., and Fallick, A.E., 2011, The Neoproterozoic Noonday Formation, Death Valley region, California: Geological Society of America Bulletin, v. 123, no. 7/8, p. 1539–1559, https://doi.org/10.1130/B30281.1.

Poole, F.G., Stewart, J.H., Palmer, A.R., Sandberg, C.A., Madrid, R.J., Ross, R.J., Jr., Hintze, L.F., Miller, M.M., and Wrucke, C.T., 1992, Latest Precambrian to latest Devonian time; development of a continental margin, *in* Burchfiel, B.C., Lipman, P.W., and Zoback, M.L., eds., The Cordilleran Orogen: Conterminous U.S.: Boulder, Colorado, Geological Society of America, The Geology of North America, v. G-3, p. 9–56, https://doi.org/10.1130/DNAG-GNA-G3.9.

Prave, A.R., Fallick, A.E., Thomas, C.W., and Graham, C.M., 2009, A composite C-isotope profile for the Neoproterozoic Dalradian Supergroup of Scotland and Ireland: Journal of the Geological Society [London], v. 166, p. 845–857, https://doi.org/10.1144/0016-76492008-131.

Pu, J.P., Bowring, S.A., Ramezani, J., Myrow, P., Raub, T.D., Landing, E., Mills, A., Hodgin, E., and Macdonald, F.A., 2016, Dodging snowballs: Geochronology of the Gaskiers glaciation and the first appearance of Ediacaran biota: Geology, v. 44, no. 11, p. 955–958, https://doi.org/10.1130/G38284.1.

Quinn, T., 1991, Meteoric diagenesis of Plio-Pleistocene limestones at Enewetak Atoll: Journal of Sedimentary Petrology, v. 61, no. 5, p. 681–703.

Sahoo, S.K., Planavsky, N.J., Kendall, B., Wang, X., Shi, X., Scott, C., Anbar, A.D., Lyons, T.W., and Jiang, G., 2012, Ocean oxygenation in the wake of the Marinoan glaciation: Nature, v. 489, p. 546–549, https://doi.org/10.1038/nature11445.

Saltzman, M.R., and Thomas, E., 2012, Carbon isotope stratigraphy, *in* Gradstein, F.M., Ogg, J.G., Schmitz, M., and Ogg, G.M., eds., The Geologic Timescale 2012, Volume 1: Amsterdam, Netherlands, Elsevier, p. 207–232, https://doi.org/10.1016/B978-0-444-59425-9.00011-1.

Sawaki, Y., Ohno, T., Tahata, M., Komiya, T., Hirata, T., Maruyama, S., Windley, B.F., Han, J., Shu, D., and Li, Y., 2010, The Ediacaran radiogenic Sr isotope excursion in the Doushantuo Formation in the Three Gorges area, South China: Precambrian Research, v. 176, p. 46–64, https://doi.org/10.1016/j.precamres.2009.10.006.

Sawyer, D.S., Swift, B.A., Sclater, J.G., and Toksöz, M.N., 1982, Extensional model for the subsidence of the northern United States Atlantic continental margin: Geology, v. 10, p. 134–140, https://doi.org/10.1130/0091-7613(1982)10<134:EMFTSO>2.0.CO;2.

Schiffbauer, J.D., Huntley, J.W., O'Neil, G.R., Darroch, S.A.F., Laflamme, M., and Cai, Y., 2016, The latest Ediacaran wormworld fauna: Setting the ecological stage for the Cambrian explosion: GSA Today, v. 26, no. 11, p. 4–11, https://doi.org/10.1130/GSATG265A.1.

Schoenborn, W.A., and Fedo, C.M., 2011, Provenance and paleoweathering reconstruction of the Neoproterozoic Johnnie Formation, southeastern California: Chemical Geology, v. 285, p. 231–255, https://doi.org/10.1016/j.chemgeo.2011.04.014.

Schoenborn, W.A., Fedo, C.M., and Farmer, G.L., 2012, Provenance of the Neoproterozoic Johnnie Formation and Stirling Quartzite, southeastern California, determined by detrital zircon geochronology and Nd isotope geochemistry: Precambrian Research, v. 206–207, p. 182–199, https://doi.org/10.1016/j.precamres.2012.02.017.

Sims, J.D., 2012, Earthquake-induced load casts, pseudonodules, ball-and-pillow structures, and convolute lamination: Additional deformation structures for paleoseismic studies, *in* Cox, R.T., Tuttle, M.P., Boyd, O.S., and Locat, J., eds., Recent Advances in North American Paleoseismology and Neotectonics East of the Rockies: Geological Society of America Special Paper 493, p. 191–201, https://doi.org/10.1130/2012.2493(09).

Smith, E.F., Nelson, L.L., Strange, M.A., Eyster, A.E., Rowland, S.M., Schrag, D.P., and Macdonald, F.A., 2016, The end of the Ediacaran: Two new exceptionally preserved body fossil assemblages from Mount Dunfee, Nevada, USA: Geology, v. 44, no. 11, p. 911–914, https://doi.org/10.1130/G38157.1.

Smith, E.F., Nelson, L.L., Tweedt, S.M., Zeng, H., and Workman, J.B., 2017, A cosmopolitan late Ediacaran biotic assemblage: New fossils from Nevada and Namibia support a global biostratigraphic link: Proceedings of the Royal Society of London, ser. B, v. 284, no. 1858, p. 20170934, https://doi.org/10.1098/rspb.2017.0934.

Steckler, M.S., and Watts, A.B., 1978, Subsidence of the Atlantic-type continental margin off New York: Earth and Planetary Science Letters, v. 41, p. 1–13, https://doi.org/10.1016/0012-821X(78)90036-5.

Stewart, J.H., 1970, Upper Precambrian and Lower Cambrian Strata in the Southern Great Basin, California and Nevada: U.S. Geological Survey Professional Paper 620, 206 p.

Stewart, J.H., 1972, Initial deposits in the Cordilleran geosyncline: Evidence of a late Precambrian (<850 m.y.) continental separation: Geological Society of America Bulletin, v. 83, p. 1345–1360, https://doi.org/10.1130/0016-7606(1972)83[1345:IDITCG]2.0.CO;2.

Stewart, J.H., and Poole, F.G., 1974, Lower Paleozoic and uppermost Precambrian Cordilleran miogeocline, Great Basin, western United States, *in* Dickinson, W.R., ed., Tectonics and Sedimentation: Society of Economic Paleontologists and Mineralogists (SEPM) Special Publication 22, p. 28–57, https://doi.org/10.2110/pec.74.22.0028.

Stewart, J.H., and Suczek, C.A., 1977, Cambrian and latest Precambrian paleogeography and tectonics in the western United States, *in* Stewart, J.H., Stevens, C.H., and Fritsche, A.E., eds., Paleozoic Paleogeography of the Western United States: Los Angeles, California, Pacific Section, Society of Economic Paleontologists and Mineralogists (SEPM), p. 1–17.

Stewart, J.H., McMenamin, M.A.S., and Morales-Ramirez, J.M., 1984, Upper Proterozoic and Cambrian Rocks in the Caborca Region, Sonora, Mexico—Physical Stratigraphy, Biostratigraphy, Paleocurrent Studies, and Regional Relations: U.S. Geological Survey Professional Paper 1309, 36 p.

Summa, C.L., 1993, Sedimentologic, Stratigraphic, and Tectonic Controls of a Mixed Carbonate-Siliciclastic Succession: Neoproterozoic Johnnie Formation, Southeast California [Ph.D. thesis]: Cambridge, Massachusetts, Massachusetts Institute of Technology, 331 p.

Swart, P.K., and Kennedy, M.J., 2012, Does the global stratigraphic reproducibility of $\delta^{13}C$ in Neoproterozoic carbonates require a marine origin? A Pliocene–Pleistocene comparison: Geology, v. 40, no. 1, p. 87–90, https://doi.org/10.1130/G32538.1.

Tahata, M., Ueno, Y., Ishikawa, T., Sawaki, Y., Murakami, K., Han, J., Shu, D., Li, Y., Guo, J., Yoshida, N., and Komiya, T., 2013, Carbon and oxygen isotope chemostratigraphies of the Yangtze platform, South China: Decoding temperature and environmental changes through the Ediacaran: Gondwana Research, v. 23, p. 333–353, https://doi.org/10.1016/j.gr.2012.04.005.

Trower, E.J., and Grotzinger, J.P., 2010, Sedimentology, diagenesis, and stratigraphic occurrence of giant ooids in the Ediacaran Rainstorm Member, Johnnie Formation, Death Valley region, California: Precambrian Research, v. 180, p. 113–124, https://doi.org/10.1016/j.precamres.2010.03.007.

U.S. Geological Survey, 1968, Mt. Schader 7.5 Minute Quadrangle, Nye County, Nevada: U.S. Geological Survey, scale 1:24,000.

Verdel, C., Wernicke, B.P., and Bowring, S.A., 2011, The Shuram and subsequent Ediacaran carbon isotope excursions from southwest Laurentia, and implications for environmental stability during the metazoan radiation: Geological Society of America Bulletin, v. 123, no. 7/8, p. 1539–1559, https://doi.org/10.1130/B30369.1.

Walker, J.D., Geissman, J.W., Bowring, S.A., and Babcock, L.E., 2013, The Geological Society of America Geologic Time Scale: Geological Society of America Bulletin, v. 125, no. 3/4, p. 259–272, https://doi.org/10.1130/B30712.1.

Wright, L.A., and Troxel, B.W., 1966, Strata of late Precambrian–Cambrian age, Death Valley region, California-Nevada: American Association of Petroleum Geologists Bulletin, v. 50, no. 5, p. 846–857.

Wright, L.A., and Troxel, B.W., 1984, Geology of the North 1/2 Confidence Hills 15′ Quadrangle, Inyo County, California: California Division of Mines and Geology Map Sheet 34, scale 1:24,000, 1 sheet, 31 p. text.

Xiao, S., Bao, H., Wang, H., Kaufman, A.J., Zhou, C., Li, G., Yuan, X., and Ling, H., 2004, The Neoproterozoic Quruqtagh Group in eastern Chinese Tianshan: Evidence for a post-Marinoan glaciation: Precambrian Research, v. 130, p. 1–26, https://doi.org/10.1016/j.precamres.2003.10.013.

Xiao, S., Narbonne, G.M., Zhou, C., Laflamme, M., Grazhdankin, D.V., Moczydlowska-Vidal, M., and Cui, H., 2016, Towards an Ediacaran time scale: Problems, protocols, and prospects: Episodes, v. 39, no. 4, p. 540–555, https://doi.org/10.18814/epiiugs/2016/v39i4/103886.

Yonkee, W.A., Dehler, C.D., Link, P.K., Balgord, E.A., Keeley, J.A., Hayes, D.S., Wells, M.L., Fanning, C.M., and Johnston, S.M., 2014, Tectono-stratigraphic framework of Neoproterozoic to Cambrian strata, west-central U.S.: Protracted rifting, glaciation, and evolution of the North American Cordilleran margin: Earth-Science Reviews, v. 136, p. 59–95, https://doi.org/10.1016/j.earscirev.2014.05.004.

Zhou, C., Xie, G., McFadden, K., Xiao, S., and Yuan, X., 2007, The diversification and extinction of Doushantuo-Pertatataka acritarchs in South China: Causes and biostratigraphic significance: Geological Journal, v. 42, p. 229–262, https://doi.org/10.1002/gj.1062.